ARNAUD CHÉRITAT

Tan Lei and Shishikura's example of non-mateable degree 3 polynomials without a Levy cycle

Tan Lei and Shishikura's example of non-mateable degree 3 polynomials without a Levy cycle

Arnaud Chéritat[1]

ABSTRACT. — After giving an introduction to the procedure dubbed *slow polynomial mating* and quickly recalling known results about more classical notions of polynomial mating, we show conformally correct pictures of the slow mating of two degree 3 post critically finite polynomials introduced by Shishikura and Tan Lei as an example of a non matable pair of polynomials without a Levy cycle. The pictures show a limit for the Julia sets, which seems to be related to the Julia set of a degree 6 rational map. We give a conjectural interpretation of this in terms of pinched spheres and show further conformal representations.

RÉSUMÉ. — Après avoir donné une introduction à la procédure baptisée *accouplement lent de polynômes* et avoir rapidement rappelé des résultats connus sur la notion plus classique d'accouplement de polynômes, nous montrons des images conformément correctes de l'accouplement lent de deux polynômes de degré 3 post critiquement finis introduits par Shishikura et Tan Lei en tant qu'exemple de paire obstruée mais sans cycle de Levy. Ces images semblent montrer que les ensembles de Julia déformés ont une limite, qui semble reliée à l'ensemble de Julia d'une application rationnelle de degré 6. Nous donnons une interprétation conjecturale de ces faits en termes de sphères pincées et montrons d'autres représentations conformes.

---

[1] Centre National de la Recherche Scientifique, Institut de Mathématiques de Toulouse, Université Paul Sabatier 118 Route de Narbonne 31062 Toulouse Cedex 9, France.
arnaud.cheritat@math.univ-toulouse.fr

Contents

1. Introduction

In [16], Tan Lei and Shishikura gave an example of two post critically finite polynomials of degree 3 whose "formal" mating has an obstruction that is not a Levy cycle.

Let us recall the context:

1.1. Context

One thing making the discussion difficult, but also interesting, is that there are several non-equivalent definitions of polynomial matings. Let us recall the definition of the slow variant (see [9] p. 54):

1.1.1. Definition of slow polynomial mating

Consider two polynomials P_1, P_2 of the same degree $d \geqslant 2$. For the construction to make sense we need that their Julia sets be connected.

Remark 1.1. — No other assumption is done. In other constructions it is either required that the Julia sets are locally connected or even stronger: that the polynomials are post-critically finite.

Recall that a polynomial of degree $d \geqslant 2$ with connected Julia set has $d - 1$ fixed external rays (i.e. of period 1). The construction that follows

depends on the choice of such an external ray for P_1, and of one for P_2. In the degree 2 case, since there is only one fixed external ray, there is no choice.
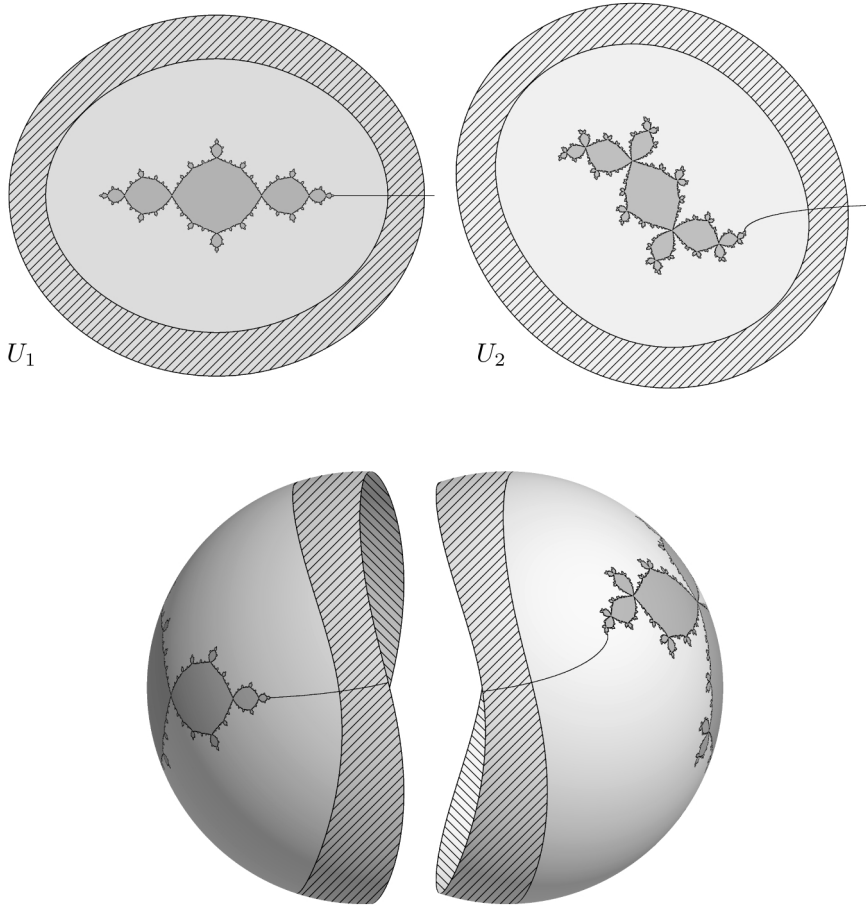
Figure 1. — Example of construction of the Riemann surface $\mathcal{S}_R$. The images depict the Julia sets nicknamed the Basilica and the Rabbit. Some value of R has been chosen and the domain bounded by the equipotential $V' > \log R$ is indicated by shades of gray. The respective external rays of argument 0 have also been drawn. The parts of U_i that get glued together are hatched. In the image below we presented the two charts facing each other in a 3D space so that points glued together are close.
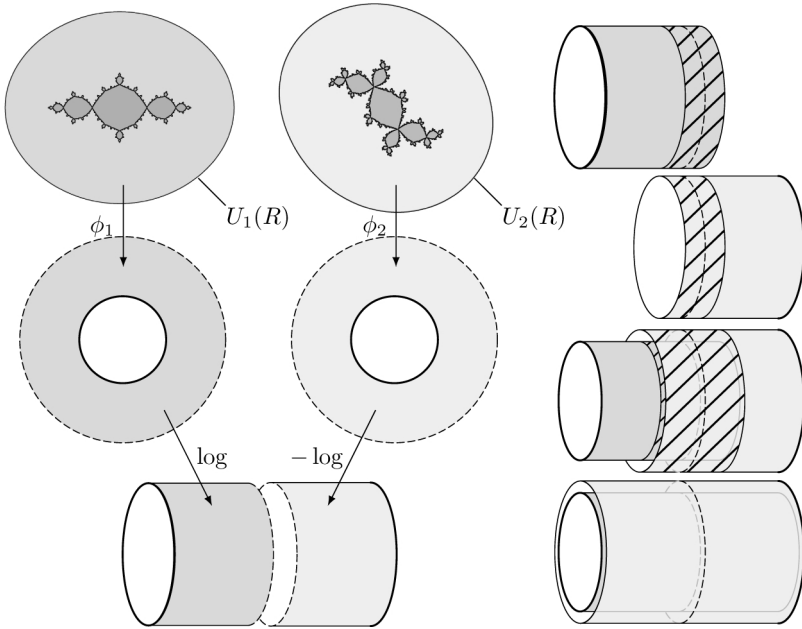
Figure 2. — Left: gluing $U_1(R)$ and $U_2(R)$ amounts to gluing their Böttcher coordinates along the circle $|z| = R$ by an inversion. Better, it is equivalent to gluing the logarithms of the Böttcher coordinates with an isometry. Right: in fact to define a Riemann surface we take slightly larger domains so that open sets are glued together. This depends on another parameter V' (with $V < V' \leqslant 2V$) which determines the overlap (the hatched parts on the tubes are glued together by an isometry). However the resulting surfaces are the same (canonically isomorphic).

For any real number $V > 0$ let $R = e^V$ and let $U_i(R)$ be the simply connected open subset of $\mathbb{C}$ bounded by the equipotential of P_i with potential V. Bascially we would like to build a Riemann surface $\mathcal{S}_R$ by gluing the closure of $U_1(R)$ and $U_2(R)$ along their boundaries in some specific fashion. Provided the gluing map is analytic, we get a Riemann surface. However we prefer to present the construction slightly differently, by gluing along open regions.

So choose $V' \in \,]V, 2V]$, and let $R' = e^{V'}$ and

$$U_i = U_i(R').$$

Now let ϕ_1 be the unique Böttcher coordinate for P_1 that maps the chosen fixed external ray to the interval $]1, +\infty[$, let ϕ_2 be the same for P_2 and

glue $z \in U_1$ with $w \in U_2$ whenever

$$\frac{\phi_1(z)}{R} \cdot \frac{\phi_2(w)}{R} = 1.$$

Note that this relation restricts to an orientation reversing bijection between the equipotentials of level V of P_1 and P_2. Note also that if $z \sim w$ then their external angles[1] are opposite. The gluing can equivalently be expressed in the coordinates $\log \phi_i$:

$$\frac{\log \phi_1(z) + \log \phi_2(z)}{2} = V \quad (\text{mod } 2\pi i).$$

It can be checked that the quotient topological space under this equivalence relation is indeed a topological manifold. Moreover, U_1 and U_2 provide an atlas for which the change of coordinates is holomorphic and thus we have defined a Riemann surface. It does not depend on the choice of $V' \in \,]V, 2V]$ in the sense that there are canonical isomorphisms between two such surfaces (see Figure 2) and will be designated as $\mathcal{S}_R$ regardless of the value of V'.
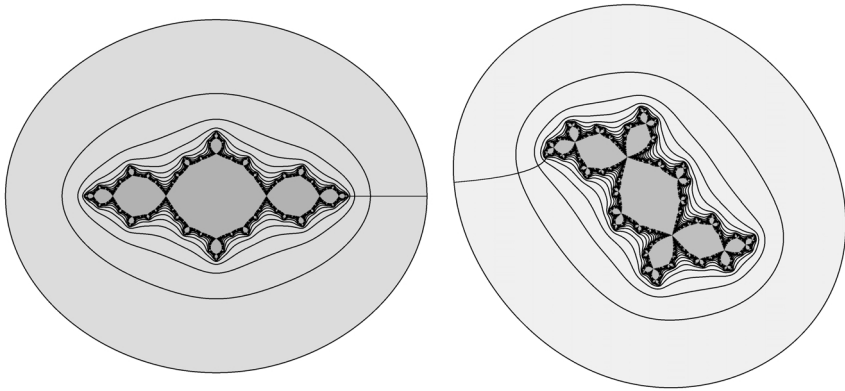
Figure 3. — Here we drew the domains bounded by the potential V together with more equipotentials. The image on the right has been rotated 180 degrees so that now the external rays of argument 0 are facing each other. On $\mathcal{S}_R$, the boundaries of these two domains are glued together and the point on the external ray 0 match. On Figure 4, we see what these pictures become after being glued to form $\mathcal{S}_R$.

----

[1] arguments of their Böttcher coordinates
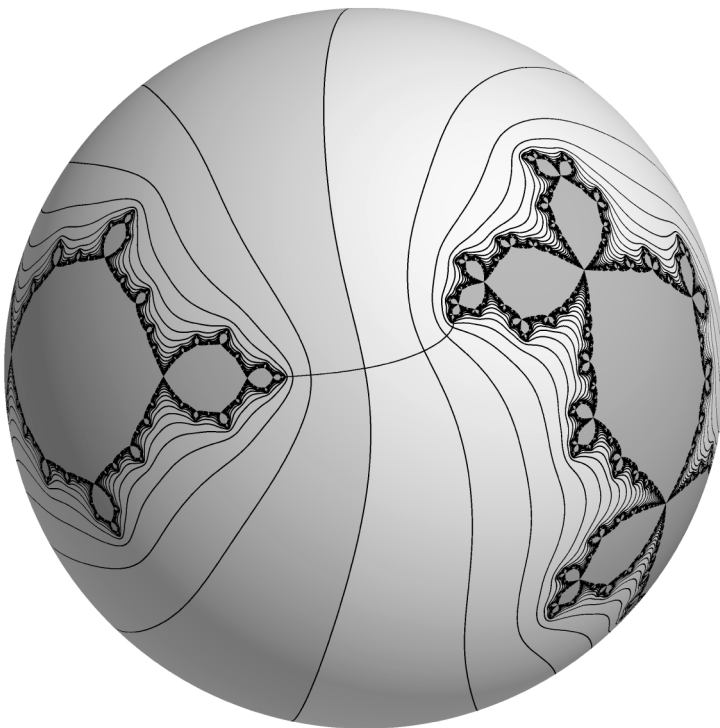
Figure 4. — The Riemann surface $\mathcal{S}_R$ conformally mapped to the Euclidean sphere, painted with the drawings of Figure 2. The method for producing such a picture is interesting and will be explained in a forthcoming article; it does not work by computing the conformal map, but instead by pulling-back Julia sets by a series of rational maps. It has connections with Thurston's algorithm.

All these surfaces are homeomorphic to the sphere, so they are isomorphic to the Riemann sphere $\widehat{\mathbb{C}}$. Recall that the latter has a group of automorphisms which is not small[2] so the isomorphism to $\widehat{\mathbb{C}}$ is not unique. Its choice will play a determinant role when we look at degenerating cases. The choice of such an isomorphism is called a normalization.

There are several objects of interest than can be defined on $\mathcal{S}_R$. First the Julia sets of P_1 and P_2 correspond to two compact subsets of $\mathcal{S}_R$. The

---

[2] It is the group of homographies a.k.a. Möbius transformations or projective self maps, i.e. those maps of the form $z \mapsto (az+b)/(cz+d)$ that are not constant. The group is also sharply 3-transitive: given a triple of pairwise distinct points a_1, a_2, a_3 in $\widehat{\mathbb{C}}$ an another one b_1, b_2, b_3 there is a unique Möbius map sending each a_i to b_i.

same holds for the filled-in Julia sets. Equipotentials and external rays are also well-defined, together with a conformal map Φ from A to the round annulus $R^{-1} < |z| < R$ where A is the the complement of the union of the two filled-in Julia sets:

$$\Phi : A \to \left\{ z \,\middle|\, R^{-1} < |z| < R \right\}.$$

Let us designate these subsets of $\mathcal{S}_R$ by $J_1(R)$, $K_1(R)$, $J_2(R)$, $K_2(R)$ and $A(R)$. The equator of $A(R)$ is the preimage of the unit circle by Φ and corresponds in either chart U_i to the equipotential $\log R$. More complicated objects can be defined. For instance the measure μ_R on the equator of $A(R)$ which is the pull-back by Φ of the uniform probability measure on the unit circle.

There is an important subtlety about the transfer to $\mathcal{S}_R$ of the dynamical system. It turns out that P_1 together with P_2 define a holomorphic map from $\mathcal{S}_R$ to $\mathcal{S}_{R^d}$, *not* to $\mathcal{S}_R$:

$$\mathcal{S}_R \xrightarrow{F_R} \mathcal{S}_{R^d}.$$

To explain this, let us recall that $R = e^V$ and $V' \in]V, 2V]$. Let $R' = e^{V'}$. Then P_i maps $U_i(R')$ to $U_i(R'^d)$ and if $z \in U_i \setminus K(P_i)$ then the Böttcher coordinate satisfies $\phi_i(P_i(z)) = \phi_i(z)^d$. Hence if the product $\phi_1(z)\phi_2(w) = R^2$ then $\phi_1(P_1(z))\phi_2(P_2(z)) = R^{2d}$. [3] If isomorphisms from $\mathcal{S}_R$ and $\mathcal{S}_{R^d}$ to $\widehat{\mathbb{C}}$ have been chosen then the holomorphic map F_R becomes a *rational map of degree d*.

Hence we get a one real parameter family of rational maps F_R of degree d between spheres with distinguished compact subsets. Note that $F_R(K_i(R)) = K_i(R^d)$, and the same holds for $J_i(R)$ and $A(R)$. Equipotentials and external rays are mapped to equipotentials and external rays.

1.1.2. Limits of slow mating?

Now, as $R \longrightarrow 1$ by values > 1, do these objects have limits? Are these limits compatible? It depends on the initial maps P_1 and P_2, but also on the meaning we give to having a limit and to compatibility. One thing we could ask for is to find a normalization of the spheres $\mathcal{S}_R$ such that the maps F_R tend to a rational map F of the same degree (which is d). We would then like both sets $J_i(R)$ to tend to the Julia set of F. We could ask more, for instance[4] that the equatorial measure μ_R tends to the Brolin-Lyubich

---

[3] In the degree 2 case it would be tempting to try to define a map from $\mathcal{S}_R$ to itself by deciding to map each half-annulus to the whole annulus. However it would be discontinuous at the equator.

[4] The author ignores if this particular requirement is implied by the previous ones.

measure of F. We could also ask for less, for instance that F_{R_n} converges for some sequence $R_n \longrightarrow 1$, or even allow F_R to tend to a lower degree map (convergence occuring on the complement of a finite set). The present article does not study these questions, it just shows an example that degenerates in a specific way.

By *slow mating* we mean the definition of the Riemann surfaces $\mathcal{S}_R$ and the objects $J_i(R)$, ..., F_R that we defined on or between them. We do not designate the (hypothetical) limit map F. Let us stress out once more that the slow mating of two polynomials of the same degree $d > 1$ is well-defined whenever both have connected Julia sets. They do not need to be post-critically finite, and the Julia sets do not even need to be locally connected. The question of the convergence of F_R can be posed in the non-locally connected case and is non-trivial. In the locally connected case, there is a notion of *topological mating*[5] obtained by gluing K_1 and K_2 along their boundaries respecting the Caratheodory loop (see [8] in the present volume for a definition), which has been proven in some cases[6] to be topologically conjugate to the limit of F_R. In the non-locally connected case, even if there is a limit, there is no notion of topological mating to which the limit could be compared.

Remark: A twist can be added to the gluing: see the end of the article by Buff, Epstein and Koch in the present volume, [2]. The real parameter $R > 1$ then becomes a complex parameter $\rho = Re^{i\theta} \in \mathbb{C} \setminus \overline{\mathbb{D}}$ and we get Riemann surfaces $\mathcal{S}_\rho$, objects $J_i(\rho)$, etc... and maps $F_\rho : \mathcal{S}_\rho \to \mathcal{S}_{\rho^d}$. We will not study this here.

Remark: Traditionally the mating of post-critically finite polynomials is not defined in terms of the slow mating but either with the topological mating (Post critically finite polynomials have locally connected Julia sets), see for instance [13] and [15], or in terms of corrected formal matings, see [16]. Relations between these notions have been studied but not completely yet. See also [2] and [3] in the present volume.

1.2. Post-critically finite polynomials

From now on, with a few explicitly indicated exceptions, we focus on the case where P_1 and P_2 are post-critically finite, abbreviated as PCF throughout this article.

---

[5] It may also be called the *instant mating* by opposition to the slow mating.
[6] A detailed discussion of this is out of the scope of the present article.

Remark 1.2. — In this article, mutlicurves will be mentioned. See [4] for a definition, or [12] in the present Volume. Many authors use the word "multicurve" for isotopy classes of these. We will not.

1.2.1. About the Thurston machinery

We recall that a PCF orientation preserving ramified self cover (continuous but not assumed holomorphic) of the (oriented) sphere is called a *Thurston map.* We assume the reader knows the definition of Thurston equivalence of Thurston maps, the definition of a Thurston map with hyperbolic orbifold, the definition of Thurston obstructions and the related existence and uniqueness theorem of rational realizations of classes of Thurston maps with hyperbolic orbifold. We do not assume the reader knows the proof, but at some point we will use Thurston's pull-back map (a.k.a. Thurston's algorithm). These subjects are discussed in details in [4]. Note that in the present article, we *do not* require an obstruction to be a *stable* multicurve.[7]

1.2.2. The marked set

In the case where P_1 and P_2 are post-critically finite, one may map the post-critical set[8] of each polynomial to $\mathcal{S}_R$ (let us call $\mathcal{P}_R \subset \mathcal{S}_R$ this finite collection of points) and try to see if these points remain at some distance from each other as $R \longrightarrow 1$ or if they will gather in different groups. It is important to stress that $\mathcal{P}_R$ is not[9] the post-critical set[10] of some $F_{R'}$. This is why we prefer to call $\mathcal{P}_R$ the *marked set.* One may try to guess the Thurston equivalence class of the limit map F of the family F_R, if any limit exists. A candidate is provided by the so-called *formal mating*, which is a Thurston map built from P_1 and P_2 (see the description in other articles in this volume, like [8] and [2]; we also give a description in Section 1.2 of the present article). In this article, it will be called the *candidate.* However there are some cases where the map F_R has a post-critically finite limit of degree d but of a different Thurston class: just because some points in $\mathcal{P}_R$ collapse at the limit does not mean that the degree drops. This case has been acknowledged and a way to correct the formal mating is known (see Section 1.3), though the author does not know if the link between corrected

---

[7] Also called invariant multicurve. A multicurve Γ for f is called stable if all components of $f^{-1}(\Gamma)$ are either peripheral or homotopic rel. the post-critical set to a curve in Γ.

[8] the union of critical values and their orbits

[9] unless accidentally

[10] However, it is the union over $n > 0$ of the critical values of the compositions $F_{R^{1/d}} \circ F_{R^{1/d^2}} \circ \cdots \circ F_{R^{1/d^n}}$

formal mating and limit of slow mating has been completely proved to hold.

1.2.3. Relation between slow mating and Thurston's algorithm

Recall that the set $\mathrm{Aut}(\widehat{\mathbb{C}})$ of automorphisms of the Riemann sphere $\widehat{\mathbb{C}}$ consists of Möbius maps. Let f be the formal mating of P_1 and P_2. It is a Thurston map defined on some oriented topological sphere S. This sphere and the post-critical set $P_f \subset S$ serve as a marker for a *Teichmüller space* $\mathcal{T}$, that plays an important role in Thurston's algorithm. We remind the reader that $\mathcal{T}$ is the set of equivalence classes, denoted $[\phi]$, of orientation preserving homeomorphisms $\phi : S \to \widehat{\mathbb{C}}$ for the relation $\phi \sim \phi'$ iff $\exists \mu \in \mathrm{Aut}(\widehat{\mathbb{C}})$ such that $\mu \circ \phi$ coincides with ϕ' on P_f and is isotopic rel P_f to ϕ' on the rest of S. Thurston's algorithm consists in the iteration of a map, the *Thurston pullback map*, which will be denoted $\sigma_f : \mathcal{T} \to \mathcal{T}$. Recall that for f PCF with hyperbolic orbifold, σ_f is weakly contracting[11] and σ_f^2 is locally strictly contracting, for some metric on $\mathcal{T}$ called the Teichmüller metric. Also, f is realizable by a rational map if and only if σ_f has a fixed point. Therefore, f is realizable if and only if $\sigma_f^n([\phi])$ has a limit in $\mathcal{T}$, and this is independent of the starting point $[\phi]$.

Now, the Riemann surfaces $\mathcal{S}_R$ defined by the slow mating come with natural[12] markings by S, i.e maps

$$\phi_R : S \to \mathcal{S}_R.$$

To specify such a marking we need to specify a construction of S and f first, and there is some flexibility in the choice. Even with a given choice, there is still some flexibility in the definition of ϕ_R. In Section 1.2, we give one example of construction with the following nice property:

$$F_R \circ \phi_R = \phi_{R^d} \circ f$$

i.e. the following diagram commutes:

$$
\begin{array}{ccc}
S & \xrightarrow{\ \phi_{R^d}\ } & \mathcal{S}_{R^d} \\
f \big\uparrow & & \big\uparrow F_R \\
S & \xrightarrow{\ \phi_R\ } & \mathcal{S}_R
\end{array}
$$

It has the following consequence: let T_R be the point in the Teichmüller

---

[11] distances are not increasing

[12] unique up to isotopy rel P_f

space $\mathcal{T}$ defined by ϕ_R. Then:[13]

$$\sigma_f(T_{R^d}) = T_R.$$

In words, this says that the slow mating defines a path $R \mapsto T_R$ in the Teichmüller space, parameterized by $R \in]1, +\infty[$, and that Thurston's pullback map associated to the formal mating acts on it as the d-th root on the parameter.

1.2.4. Squeezing the annulus

In this section we do not need the polynomials P_1 and P_2 to be PCF, we just require them to have connected Julia sets. Given two values R, R' it is quite natural to define the following non-holomorphic map:[14]

$$\Psi_{R',R} : \mathcal{S}_R \to \mathcal{S}_{R'}$$

defined as folows: map $z \in K_1$ in the chart $U_1(R)$ to the point of $\mathcal{S}_{R'}$ with the same coordinate z in $U_1(R')$. Do the same for K_2. Map a point in the annulus $A(R)$ to the point on the same external ray but with potential multiplied by $\log R'/\log R$ (the potential may be measured in either the Böttcher coordinates of P_1 or that of P_2, or also with $\log|\Phi|$ that assigns 0 to the equator, where Φ is the isomorphism from $A(R)$ to $1/R < |z| < R$; in all cases this gives the same result). This map is continuous and better: it is quasiconformal.

These maps are compatible with the dynamics:

$$F_{R'} \circ \Psi_{R',R} = \Psi_{R'^d,R^d} \circ F_R$$

i.e. the following diagram commutes:

$$
\begin{array}{ccc}
\mathcal{S}_{R^d} & \xrightarrow{\Psi_{R'^d,R^d}} & \mathcal{S}_{R'^d} \\
F_R \uparrow & & \uparrow F_{R'} \\
\mathcal{S}_R & \xrightarrow{\Psi_{R',R}} & \mathcal{S}_{R'}
\end{array}
$$

and

$$\Psi_{R'',R} = \Psi_{R'',R'} \circ \Psi_{R',R}.$$

On the annuli $A(R)$, $A(R')$, ..., these two identities basically follow from the fact that F and Ψ act as multiplications on the potential and on the external angle, and multiplications commute.

---

[13] Note that such a strong property as $F_R \circ \phi_R = \phi_{R^d} \circ f$ is not necessary to get $\sigma_f(T_{R^d}) = T_R$: a Thurston equivalence $\phi_{R^d}^{-1} \circ F_R \circ \phi_R \sim f$ would have been enough. However, it is as easy to directly get a ϕ_R satisfying the strong assumption.

[14] Note the inversion: it will make equations described later easier to handle; it is regrettable but almost imposed on us by the fact that the composition notation $f \circ g$ reads backwards.

1.2.5. A construction of the formal mating and of markings of $\mathcal{S}_R$

In fact we will give two. In this section we do not need the polynomials P_1 and P_2 to be PCF, we just require them to have connected Julia sets.

The quick and dirty way consists in choosing a particular value of R, say $R = \exp(1) = e$ and using $S = \mathcal{S}_e$, $f = \Psi_{e,e^d} \circ F_e$, and letting the marking be: $\phi_R = \Psi_{R,e}$. The claims of Section 1.2 follow at once.

For the second construction, map $\mathbb{C}$ to the unit disk by the non-conformal homeomorphism $\psi : z \mapsto z/(1 + |z|)$. Let S be the quotient of the disjoint union of two copies $\overline{D}_1$ and $\overline{D}_2$ of the closed unit disk, glued along their boundaries with $e^{i\theta} \in \partial D_1$ identified with $e^{-i\theta} \in \partial D_2$. We will identify $\overline{D}_1$ and $\overline{D}_2$ with their image in S. We first define a modification of P_1, call it $\widetilde{P}_1$ as follows: $\widetilde{P}_1 = P_1$ on K_1 and for $z \in \mathbb{C} \setminus P_1$, $\widetilde{P}_1(z)$ is the point of $\mathbb{C} \setminus K_1$ with the same potential as z, but with external angle multiplied by d. The map $\widetilde{P}_2$ is defined similarly. Then let f be the conjugate of $\widetilde{P}_1$ by ψ on D_1, the conjugate of $\widetilde{P}_2$ by ψ on D_2 an be the multiplication by d of the argument on the circle bounding D_1 and D_2. Now for $z \in S$ let $\phi_R(z)$ be defined as follows. If $z \in D_1$ then let $w = \psi^{-1}(z) \in \mathbb{C}$; if $w \in K(P_1)$ then let $\phi_R(z)$ be the point of coordinates w the chart U_1; if $w \notin K(P_1)$ then let V be the potential of w (it can be any real number in $]0, +\infty[$ since w can be any complex number in $\mathbb{C} \setminus K(P_1)$) and let $\phi_R(z)$ be the point in the chart $U_1(R)$ whose coordinate is the point on the same external ray of P_1 as w, but with potential $\log(R)V/(1 + V)$.

Remark 1.3. — In both cases we chose the markings so that

$$\phi_{R'} = \Psi_{R',R} \circ \phi_R.$$

Such a strong property was not necessary. Note also that, as far as the Thurston characterization of rational functions is concerned, the particular dynamics of f is not relevant, only its Thurston equivalence class is. Other constructions exist, for instance one where the map f is C^∞ on a C^∞ sphere, and has an attracting equator. In the latter case, the markings cannot satisfy both $\phi_{R'} = \Psi_{R',R} \circ \phi_R$ and $\phi_{R^d}^{-1} \circ F_R \circ \phi_R = f$, but they still satisfy the following weaker form: $\phi_{R^d}^{-1} \circ F_R \circ \phi_R$ is isotopic to f by an isotopy that does not move points in K_1 and K_2. If P_1 and P_2 are PCF, this weak form nonetheless implies that $\phi_{R^d}^{-1} \circ F_R \circ \phi_R$ and f are Thurston equivalent.

1.3. Topological mating vs formal mating

This section will mention the notions of *topological mating* and *ray equivalence classes*. They are discussed in details in the present volume in [8].

Note that when the topological quotient space $S/\sim$ in the definition of topological mating is homeomorphic to the sphere, there is a well-defined preferred orientation: indeed the choice of an orientation on a space X homeomorphic to the sphere induces a choice of isomorphism of its first singular homology group $H_1(X)$ to $\mathbb{Z}$. Having chosen an orientation on S, we choose the orientation on the quotient so that the quotient map $S \to S/\sim$ induces the identity $\mathbb{Z} \to \mathbb{Z}$.

Assume that P_1 and P_2 are PCF. It may happen that some ray equivalence classes contain several marked or critical points. Then the topological mating cannot be Thurston equivalent to the formal mating: the formal mating has to be corrected. Rees, Shishikura and Tan Lei have devised at least three ways of doing it, which probably have been proven equivalent (though the author could not find a written proof): see [13], [15] and [16]. In [15], it is proven that if the corrected formal mating in the sense of [15] exists and is realizable (Thurston-equivalent to a rational map) then the topological mating is conjugate to the same rational map. The converse of this statement reads: if the topological mating of two post-critically finite polynomials is conjugate to a rational map F then the corrected formal mating in the sense of [15] exists and is Thurston-equivalent to F. It has been proven by Rees in the case that the two polynomials are hyperbolic (see [13]), in which case the formal mating does not need correction. The author thinks that the converse also holds for any pair of post-critically finite polynomials, though he could not find a written proof of it. It should follow from the following theorem of Moore (see [8] for instance): if S is the 2-dimensional sphere and $\phi : S \to S$ is continuous, surjective, with connected fibers, then ϕ is the uniform limit of a sequence of homeomorphisms.

Even in degree 2, there are pairs of post-critically finite polynomials which have an obstructed formal mating but still have a topological mating conjugated to a rational map: for instance the mating, studied in [10], of $P = z^2 + c$ with itself where c is at the end of the Mandelbrot set external ray of argument $1/4$. The post-critical set of $P_1 = P_2 = P$ has three elements: $P(c), P^2(c), P^3(c) = P^4(c)$. The ray equivalence identifies $P_1^2(c)$ with $P_2^2(c)$ and $P_1^3(c)$ with $P_2^3(c)$, but no other point in the post-critical set of P_1 and P_2. Their topological mating is conjugate to the non-flexible Lattès map associated to multiplication by $1 + i$ on the square lattice.

Note that the slow mating is a realization of the Thurston algorithm for the formal mating but not for the corrected formal mating. In the case of a mating that needs and has a correction, it is likely that under the slow mating, the marked points belonging to a same ray class will get closer and

closer and tend to a single point[15], and that the maps F_R will converge to a map of the same degree (i.e. without loss of degree). We do not know if it has been proved completely.

1.4. Levy cycles

In his thesis [7], Silvio Levy proved the following theorem. Let f be a post-critically finite topological ramified self-cover of the sphere:

THEOREM 1.4 (Levy). — *If f has degree 2 then it has a Thurston obstruction if and only if it has a Levy cycle.*

A Levy cycle is a numbered multicurve $\gamma_0, \gamma_1, \ldots, \gamma_n = \gamma_0$ such that for all k, γ_{k+1} is isotopic rel. P_f to a component of $f^{-1}(\gamma_k)$ on which f has degree 1, see [8] in this volume The curves of a Levy cycle form an obstruction so one implication of the theorem is trivial. Note that the Levy character of a given numbered multicurve cannot be read off from its Thurston matrix.[16]

1.4.1. Polynomial matings and Levy cycles

Formal matings which need and have a correction have a special class of Levy cycles called removable Levy cycles.

Concerning matings of post-critically finite polynomials, the situation is completely understood in degree 2: using Levy's theorem, Tan Lei proved:

THEOREM 1.5 (Tan Lei). — *The pairs of post-critically finite polynomials of degree 2 whose topological mating is not equivalent to a rational map are those who belong to conjugate limbs of the Mandelbrot set. Moreover, their ray equivalence classes contain loops and the quotient topological space in the definition of the topological mating is not a sphere.*

However, not only Levy's theorem has counter examples in degree $\geqslant 3$ but it is has counter examples among formal matings:

THEOREM 1.6 (Shishikura, Tan Lei, [16]). — *There exist a pair of post-critically finite polynomials of degree 3 whose formal mating is obstructed*

---

[15] In the sense that they will be separated from the other marked points by an annulus of modulus tending to $+\infty$ separating them from the others, or equivalently by a geodesic of length tending to 0, for the hyperbolic metric on the complement of the marked points: see Section 1.4

[16] There exists a pair of maps each with a multicurve with the same matrix, but one multicurve is a Levy cycle and the other is not. This is because the coefficients in the matrix are sums of inverse of integers, and one cannot deduce the presence of the term 1 from the value of the sum.

but has no Levy cycles. Moreover, the corresponding quotient topological space is homeomorphic to a sphere.

Having no Levy cycles, this mating is not correctable, so the topological mating of P_1 and P_2 is not conjugate to a rational map. The author believes one can prove it implies there is no way to normalize the spheres $\mathcal{S}_R$ so that the rational maps F_R converge uniformly as $R \longrightarrow 1$, even for a subsequence $R_n \longrightarrow 1$. In this particular example, this is supported by the experiments presented in Section 2. It is remarkable, though, that the quotient topological space is still a sphere: this is basically because the ray equivalence relation is closed and the classes contain no loop (see [16]).

1.4.2. Description of the example of Tan Lei and Shishikura

Their example is an explicit pair of post critically finite polynomials (P_1, P_2) that we will define now.

Post-critically finite polynomials can be characterized, up to complex-affine conjugacy, by the augmented Hubbard trees. Recall that the augmented Hubbard tree is the Hubbard tree together with some angle information at some vertices.[17] Remember also that to mate polynomials, we must align the external angles. This can be done by choosing which fixed external ray is the one of angle 0 (this amounts to choosing monic centered polynomials). In terms of the combinatorial information, this means giving some enough supplementary information to distinguish it.[18]

It turns out that less information is often sufficient. Here the polynomials P_1 and P_2 in the example of Tan Lei and Shishikura can be charaterized up to $\mathbb{C}$-affine conjugacy by the data on Figure 5. The monic centered polynomials are uniquely determined by the data on Figure 6. In particular P_1 has critical points x, y and a 3-cycle $x \mapsto y \mapsto z \mapsto x$, and P_2 has a double critical point (thus of local degree 3) of period 3. The notations x, y, z are that of [16]; in the present article, these points will be denoted x_0, y_0 and y_1.

---

[17] Explanation: by uniqueness in Thurston's theorem, a polynomial will be characterized, up to $\mathbb{C}$-affine conjugacy, by its Thurston class. It is well known that the Hubbard tree is not enough for characterizing the Thurston class. In fact, once one has the tree H, one can characterize its first preimage H' by P up to homeomorphism of the plane. The problem is then to determine how H is embedded in H', and there may be several inequivalent ways for a fixed H, even taking the dynamics on H into account. Supplementary information is needed to determine this. The augmented Hubbard tree gives sufficient information.

[18] This is not very important, but note that for polynomials commuting with a rotation, one only needs to characterize a class of fixed external ray modulo this rotation.
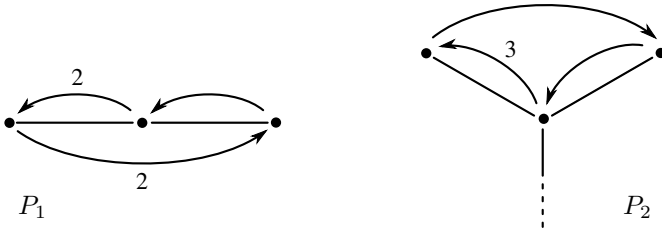
Figure 5. — Hubbard trees H of P_1 and P_2. The number over the arrow indicates the local degree at the starting point when it is not one. The dashed line indicates how some particular edge of the first preimage of H branches on H.
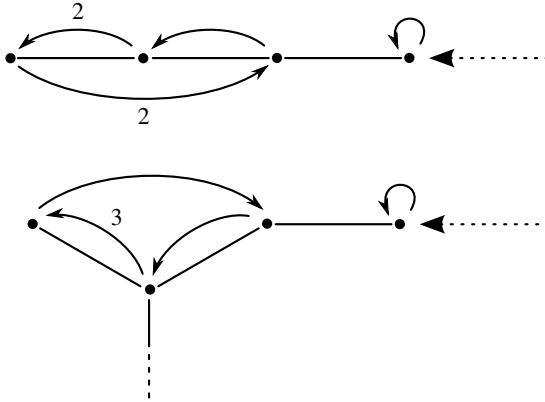

Figure 6. — Here we added the endpoint of the external ray $\mathcal{R}$ of angle 0 of each monic polynomial, together with $\mathcal{R}$ pictured with dotted arrows. This data is enough, at least on these examples, to uniquely determine the monic centered polynomials P_1 and P_2. We did not indicate the other fixed external ray, which has angle 1/2.

The polynomials are

$$\begin{aligned}
P_1(z) &= z^3 + az + b \\
P_2(z) &= z^3 + c
\end{aligned}$$

with

$$a = -3x_0^2, \quad b = 2x_0^3 - x_0, \quad 32x_0^8 - 24x_0^6 + 2x_0^2 - 1 = 0, \quad x_0 \approx 0.8445,$$
$$c^8 + 3c^6 + 3c^4 + c^2 + 1 = 0, \quad c \approx -0.264 + 1.260i.$$

And their Julia sets are illustrated on Figure 7.

y_0

x_0
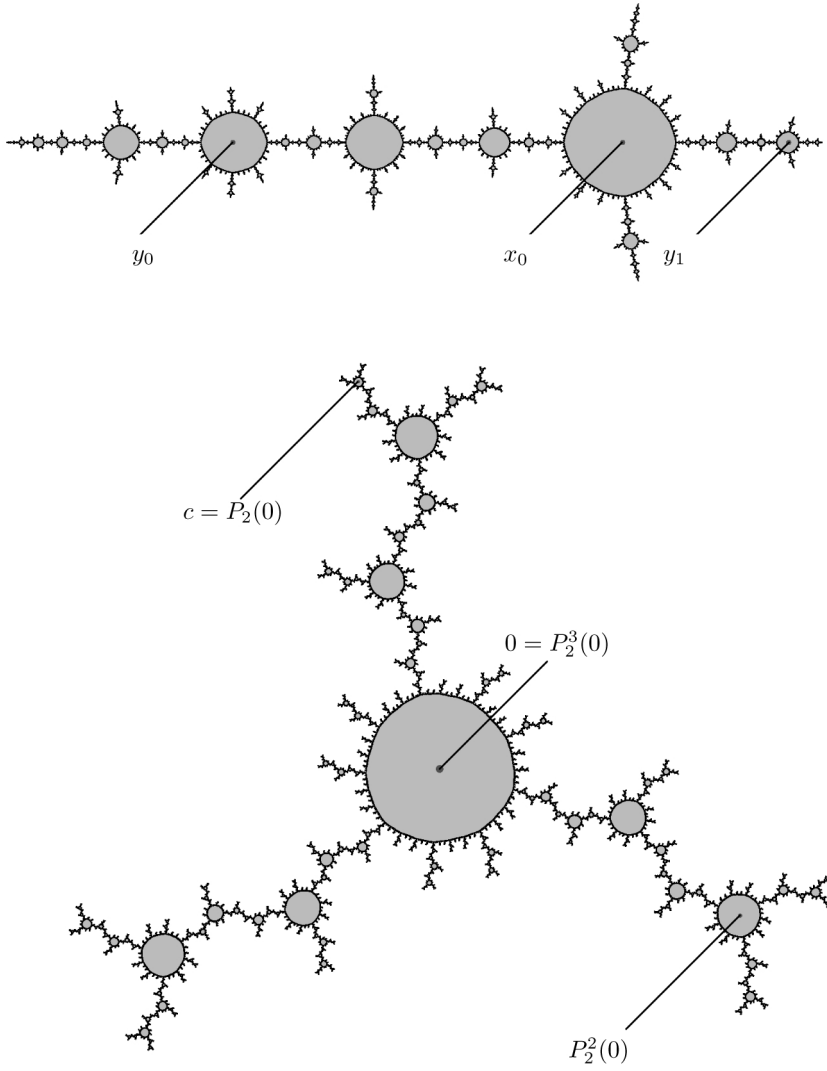
y_1

$c = P_2(0)$

$0 = P_2^3(0)$

$P_2^2(0)$

Figure 7. — The Julia sets of P_1 and P_2.
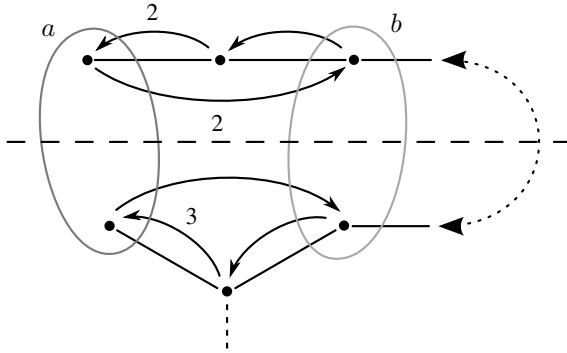
1.4.3. An obstruction for the example

Figure 8. — The multicurve $\{a, b\}$ is an obstruction for the formal mating of P_1 and P_2. The horizontal dashed line represents the equator and the dotted line the external angle of argument 0. The vertical dashed line is the same as on Figure 5.
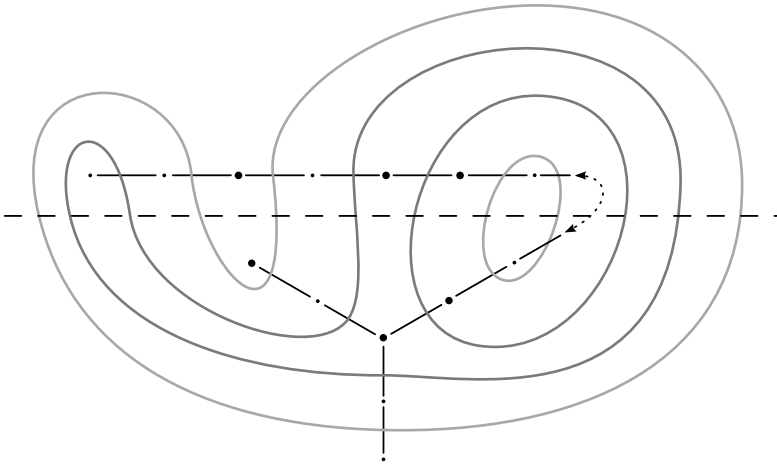

Figure 9. — Preimage by the formal mating of the multicurve $\{a, b\}$ and of the Hubbard trees. The external ray of angle 0 is also indicated. Big dots represent the marked points, i.e. the post-critical set of the formal mating f. Here, the preimage of the big dots by f is the union of the big and the small dots.

The formal mating f has a Thurston obstruction, a multicurve $\Gamma = \{a, b\}$, illustrated on Figure 8. On Figure 9 we put the preimage of Γ. From this it is easily seen that the Thurston matrix associated to Γ in the basis (a, b) is:

$$\begin{bmatrix} 1/2 & 1/2 \\ 1 & 0 \end{bmatrix}.$$

This matrix has spectrum $\{-1/2, 1\}$ therefore Γ is indeed an obstruction.

1.4.4. About pinching curves

This section may be skipped by the reader familiar with the theory. The interested reader may look at [5] or [1].
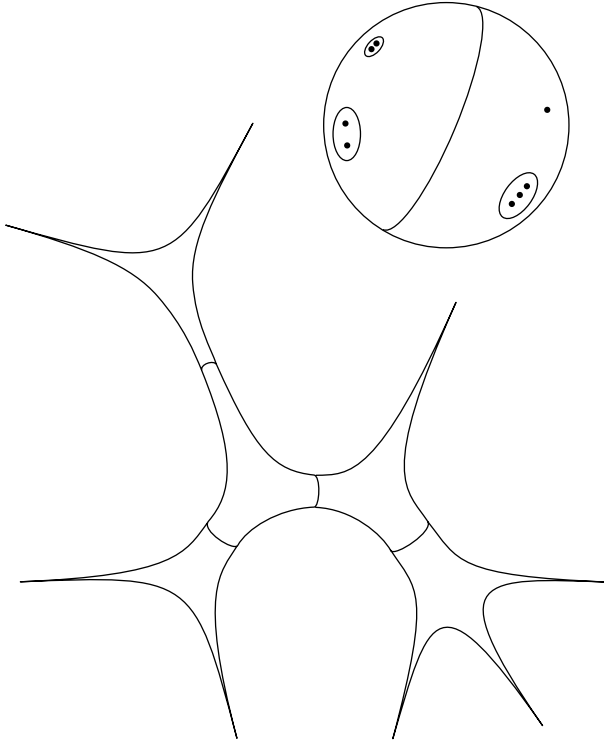

Figure 10. — A configuration of points on the Riemann sphere $\widehat{\mathbb{C}}$, together with a multicurve, supposedly homotopic to the short geodesics. Below it, a representation of what the hyperbolic metric should look like; the 8 cusps correspond to the 8 marked points, and they are infinitely long.
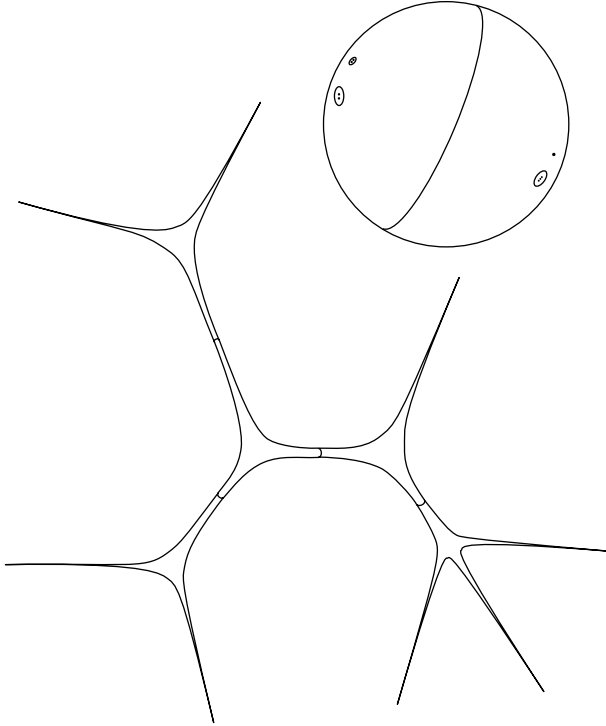
Figure 11. — Same object but with shorter geodesics. The hyperbolic version is represented with a bigger scale than on the previous figure. This picture and the previous one are not meant to be precise, but to give a sense of the hyperbolic metric.

We denoted earlier $f : S \to S$ the formal mating and P_f its postcritical set. Recall: a point $[\phi]$ in the Teichmüller space $\mathcal{T} = \mathcal{T}(S, P_f)$ is an equivalence class of map $\phi \to \widehat{\mathbb{C}}$ for the appropriate equivalence relation. The elements of $\phi(P_f)$ are called the marked points. Thurston's pull-back map associates to $[\phi]$ a new point $\sigma_f([\phi])$.

The *moduli space* $\mathcal{M}(P_f)$, more tractable in many respects, is the set of maps from P_f to $\widehat{\mathbb{C}}$ modulo post-composition by a Möbius map. We will call its elements *configurations*. There is a projection $\pi : \mathcal{T}(S, P_f) \mapsto \mathcal{M}(P_f)$ that maps the class of ϕ to the class of its restriction to P_f. The following proposition is important in the theory of Thurston's pull-back map: if a Thurston map f has hyperbolic orbifold, then $\sigma_f^n([\phi])$ diverges in $\mathcal{T}(S, P_f)$ if and only if $\pi(\sigma_f^n([\phi]))$ leaves every compact of $\mathcal{M}(P_f)$. Thus, no matter what normalization one chooses, for the configuration of points on $\widehat{\mathbb{C}}$ given

by $\pi(\sigma_f^n([\phi]))$, after passage to a subsequence, there will be at least two points with the same limit.

The fact that one has normalizations to choose makes the discussion difficult and it is much more pleasant to work with the more rigid structure provided by the hyperbolic metric, a.k.a. Poincaré metric, of the complement of the marked points, i.e. of $U = \widehat{\mathbb{C}} \setminus \phi(P_f)$. We will explain why. Before, let us state here a few facts concerning the geometry of the Poincaré metrics (see [5]).

First fact. In each of the two components of the complement in $\widehat{\mathbb{C}}$ of a simple closed geodesic in U, there are at least two marked points. Conversely, for each simple closed curve γ in U such that both components of $\widehat{\mathbb{C}} \setminus \gamma$ contain at least two marked points (such curves are called *non-peripheral*), there is a unique geodesic homotopic to γ (and it is the shortest curve homotopic to γ).

Second fact. Endow temporarily $\widehat{\mathbb{C}}$ with a spherical metric, using for instance a stereographic projection from the Euclidean 2-sphere. There exists a map $h(\varepsilon) \underset{\varepsilon \to 0}{\longrightarrow} 0$ such that for a configuration $C \in \mathcal{M}(P_f)$ with a simple closed geodesic of hyperbolic length $\leqslant \varepsilon$, whichever representative (normalization) $\phi \in C$ is chosen, there is at least one side of the geodesic where the marked points are grouped in a cluster of spherical diameter at most $h(\varepsilon)$, and there exists $\phi \in C$ such that both groups live at spherical distance $\leqslant h(\varepsilon)$ of respectively 0 and ∞. Conversely there is a map $g(\varepsilon) \underset{\varepsilon \to 0}{\longrightarrow} 0$ such that if $C \in \mathcal{M}(P_f)$ has a representative for which the marked points are split in two groups, each with at least two points, and one at spherical distance $\leqslant g(\varepsilon)$ from 0 and the other at spherical distance $\leqslant g(\varepsilon)$ from ∞, then there is a simple closed geodesic separating the groups and of hyperbolic length $< \varepsilon$ in U.

As a corollary: a sequence of configurations $[\phi_n] \in \mathcal{M}(P_f)$ will leave every compact in $\mathcal{M}(P_f)$ if and only if there exists a sequence of simple closed geodesics γ_n in $U_n = \widehat{\mathbb{C}} \setminus \phi_n(P_f)$ whose lengths tend to 0.

Third fact. Two disjoint non-peripheral curves are homotopic to geodesics which are either disjoint or equal. In particular a multicurve in $U = \widehat{\mathbb{C}} \setminus \phi(P_f)$ has a privileged representative, which is the collection of simple closed geodesics homotopic to its curves.

Fourth fact. There is a universal constant $L_0 > 0$ such that no two different geodesics of length $< L_0$ can intersect (also, but we will not use this fact, a closed geodesic with length $< L_0$ is necessarily simple). If P_f

has k points then there are at most $k - 2$ different simple closed geodesics of length $< L_0$.

Pieces: Hence endowing $\widehat{\mathbb{C}} \setminus \phi(P_f)$ with its hyperbolic metric, gives us a way to separate the marked points into groups, by cutting the sphere along those few simple closed geodesics that are small (with a notion of small chosen according to the use, for instance shorter than L_0). In fact we get more than just groups of points: all pieces do not necessary contain a marked point; the graph whose vertices are pieces and edges are curves separating two pieces is a tree. See Figures 10 and 11.

Tree: More generally cut a sphere with marked points along a multicurve. The sphere is split into open pieces U_i. Let U_i' be the pieces minus the marked points. Each U_i' has at least three boundary components, which may be points or curves. Sometimes, there are no points in some pieces U_i. Nevertheless, it is possible to single out any U_i by choosing three marked points. More precisely, for any three marked points, there is a unique U_i' which, when removed from the sphere, disconnects the three points (this is related to the tree structure associated to the pieces). For every component, there is a (not necessarily unique) set of three points that it disconnects.
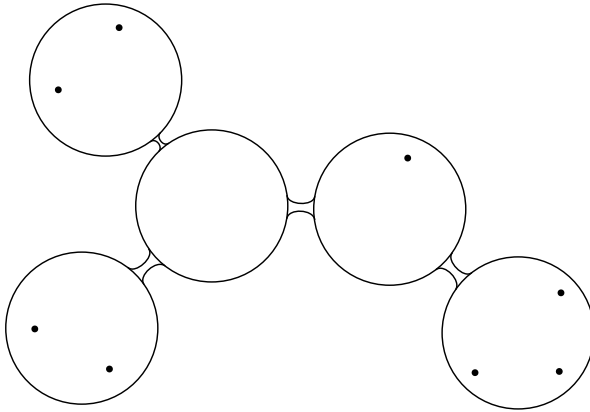

Figure 12. — Another (schematic) conformal model of the punctured sphere with short geodesics: a tree of spheres. A Möbius map will zoom on each piece, represented here as a sphere. By removing carefully chosen small disks from each sphere and adding tubes to link them together, one can recover a punctured Riemann surface that is isomorphic to the punctured sphere under consideration. Note that there is flexibility in the choice of the sizes of the removed disks and in the choice of the shapes of the tubes.
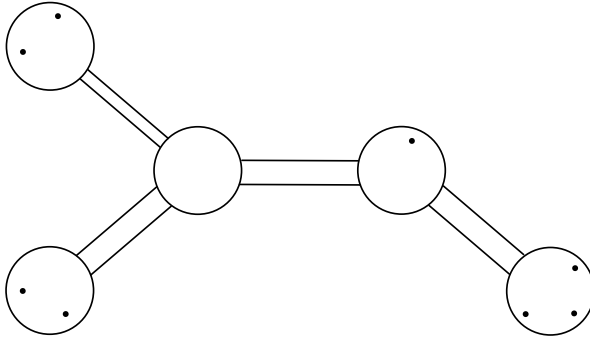
Figure 13. — Yet another conformal model.

Zoom: Let us get back to $\widehat{\mathbb{C}} \setminus \phi(P_f)$ with its conformal structure and its hyperbolic geometry. Cut it along small simple closed geodesics (the meaning of the word "small" depends on the practical application). Select three marked points, with some order, and compose ϕ with the unique Möbius map sending them respectively to 0, 1, ∞. This normalization gives a new representative of the configuration which focuses (or kind of zooms) on the piece associated to the selected triple. The smaller the geodesics bounding the piece, the more concentrated the marked point on the other side of the geodesic, viewed on the normalized Riemann sphere.

Figure 12 sums this up by a conformal presentation of the Riemann surface taking pinching curves into account. These trees of spheres are the usual point of view used for the definition of a standard compactification of the moduli space, see [1]. Figure 13 gives yet another way to conformally represent things. It puts the emphasis both on the sphere and on the funnels between them. The latter are annuli with big moduli, so they can also be viewed as tunnels. Later we will present some conformally accurate images that focus on a tunnel instead of focusing on the big spheres.

1.4.5. The canonical obstruction

Let us say that two simple closed curves γ and γ' in $\widehat{\mathbb{C}} \setminus P_f$ are homotopically transverse if there is no curve homotopic to γ and disjoint from γ'. Kevin Pilgrim in [11] precised how the curves pinch under iteration of Thurston's pull-back map:

THEOREM 1.7 (Pilgrim). — *If f is Thurston map with hyperbolic orbifold and is not realizable (so it has obstructions), then there exists a multicurve Γ, whose isotopy class is called the* canonical obstruction, *such that* $\forall [\phi] \in \mathcal{T}$, *let* $[\phi_n] = \sigma^n([\phi])$ *and* $U_n = \widehat{\mathbb{C}} \setminus \phi_n(P_f)$:

- Γ *is not empty,*

- *for all curve $\gamma \in \Gamma$, the (simple closed) geodesic in U_n homotopic to $\phi_n(\gamma)$ has a length tending to 0 as $n \longrightarrow +\infty$,*

- $\exists N \in \mathbb{N}$ *and $L > 0$ such that $\forall n \geqslant N$, these geodesics are the only simple closed geodesics shorter than L,*

- Γ *is an obstruction,*

- Γ *is f-stable and surjective[19],*

- *no curve in any obstruction can be homotopically transverse to a curve of Γ,*

The canonical obstruction is unique (as an isotopy class).

It shall be emphasized that there exists examples with hyperbolic orbifold having obstructions that do not pinch. Still, these examples have canonical obstructions that do pinch.

One last remark: even though the hyperbolic geometry is a pleasant way to formulate things, the core of the proofs of Thurston's and Pilgrim's theorems use moduli of annuli, and this language could have been used instead.

1.4.6. Does the obstruction pinch?

We prove in this section that in the example of Shishikura and Tan Lei, the given obstruction $\Gamma = \{a, b\}$ is the canonical obstruction.

In all this section, homotopic means homotopic in the complement of P_f and isotopic means isotopic rel. P_f.

LEMMA 1.8. — *Let γ be a non-peripheral simple closed curve disjoint from a and b. Then all components γ' of $f^{-1}(\gamma)$ are either peripheral or homotopic to a or b.*

---

[19] Surjective (non official terminology): It means that all curve in γ is homotopic to at least one curve in $f^{-1}(\Gamma)$. To a multicurve is associated a directed graph with vertices the curves and arrows $a \to b$ whenever b is homotopic to a component of $f^{-1}(a)$. The multicurve is called surjective whenever all b have an incoming arrow, in analogy to functions. It does not imply that the matrix is surjective.
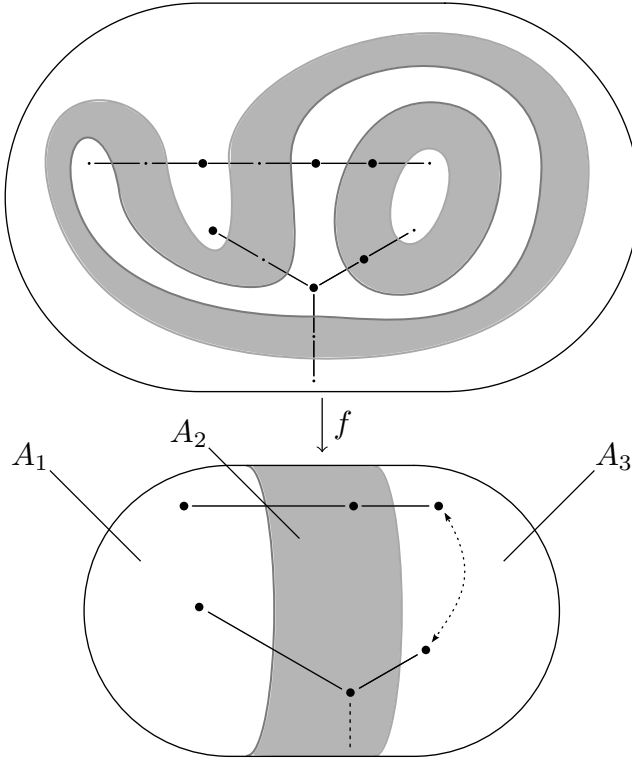
Figure 14. — Illustration for Lemma 1.8.

Proof. — The multicurve $\Gamma = \{a, b\}$ cuts the sphere into three parts A_1, A_2, A_3, each of which contains exactly two marked points. The curve a separates A_1 from A_2 and b separates A_2 from A_3. See Figure 14. The curve γ is contained in one of these components.

1. If $\gamma \subset A_1$, since $A_1 \setminus P_f$ only has three boundary components, which are two marked points and the curve a, all non homotopically trivial simple closed curve in $A_1 \setminus P_f$ is either homotopic to a small loop around a marked point, and thus peripheral, or homotopic to a. In particular γ is homotopic to a. The preimage of a has two components, one homotopic to a and the other to b.

2. Similarly, if $\gamma \subset A_3$, then it is homotopic to b, which has two preimages, one homotopic to a and the other which is homotopically trivial.

3. Last, if $\gamma \subset A_2$, note that A_2 has two preimages by f, one which is an annulus containing no marked points and whose equator is homotopic to a, and one which is an annulus containing two marked point and isotopic to a subset of A_3. If γ' is contained in the first one, it is either null-homotopic or homotopic to a. If γ' is contained in the second one, then it is homotopic via the isotopy to a curve contained in A_3, and by the same arguments as above, it is thus either peripheral or homotopic to b.

□

Let $\mathcal{C}$ be the union of the homotopy classes in the canonical obstruction. Denote $\gamma \to \gamma'$ whenever γ' is homotopic to a component of $f^{-1}(\gamma)$. Note that the arrow goes in the opposite direction to that of f. Surjectivity of the canonical obstruction tells that all curves $\gamma \in \mathcal{C}$ are homotopic to a component of the preimage of a curve in $\mathcal{C}$. By the last item of Theorem 1.7, this component has a representative disjoint from a and b. Since γ is not peripheral, the lemma tells us $\gamma \sim a$ or $\gamma \sim b$. So the canonical obstruction is homotopically contained in Γ. Moreover since the canonical obstruction is not empty, a or b must be in $\mathcal{C}$. Last, by f-stability, and since $a \to b$ and $b \to a$, we know that a and b belong to $\mathcal{C}$. So Γ is the canonical obstruction.

2. Conformal limit of the example of Shishikura and Tan Lei

In this section we show conformally accurate pictures of the slow mating on the Riemann sphere. We then give a conjectural explanation of what is going on, and finish with a few more pictures.

2.1. Conformally correct computer generated pictures

We need to give practical labels to the post-critical points of the formal mating f and to the marked points. Let x_0 and y_0 denote the critical points of f corresponding to the critical points x_0 and y_0 of P_1. Let y_1 be the point corresponding to $P_1(y_0)$. Recall that $x_0 \mapsto y_0 \mapsto y_1 \mapsto x_0$. Let c_0 denote the critical point of f corresponding to the critical point 0 of P_2. Let c_1 and c_2 correspond to $c = P_2(0)$ and $P_2^2(0)$. Recall that the marked points on $\mathcal{S}_R$ are the images of the post-critical points of f by the marking $\phi_R : S \to \mathcal{S}_R$. We will use the same labels for the marked points as for the post-critical points of f.
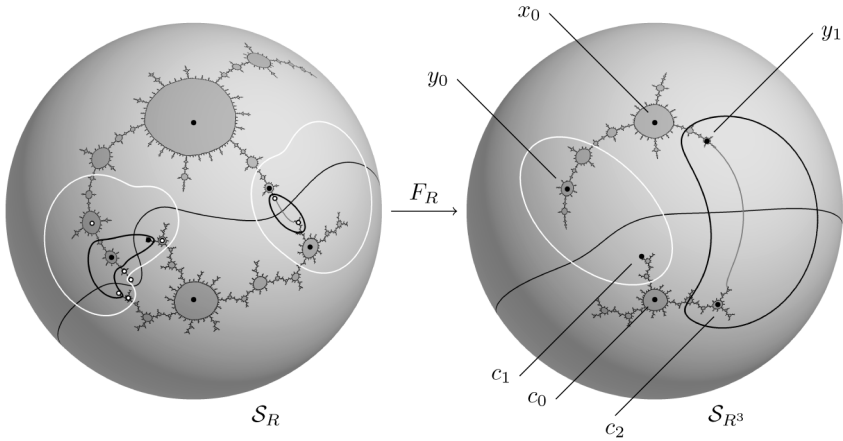
Figure 15. — Conventions: In both pictures, the gray line is the external ray of argument 0 and the black dots are the marked points. On the right, the multicurve $\{a, b\}$ is drawn with a in white and b in black. On the left we drew the (accurate) preimage of the right by F_R. The white dots indicate those preimages of the black dots that are not themselves marked. Here, $R \approx 1.41$, $R^3 \approx 2.78$.
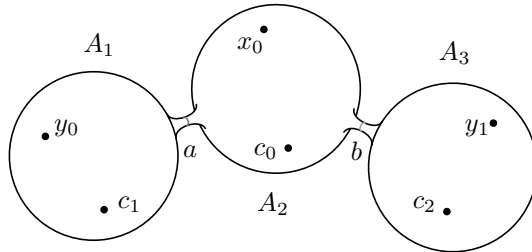

Figure 16. — A pinched sphere model of $\mathcal{S}_R$ for R close to 1.

On Figure 15 we drew the spheres $\mathcal{S}_R$ for a pair of values R and R^3, together with the Julia sets and the equator. We also drew a multicurve[20] corresponding to the obstruction $\Gamma = \{a, b\}$ and its preimage by F_R.

In Section 1.4 we proved that the canonical obstruction is $\Gamma = \{a, b\}$. Thus as $R \longrightarrow 1$, the marked sphere will be conformally equivalent to something looking like Figure 16.

---

[20] Multicurves are usually defined for Thurston maps $f : S \to S$ but in the proof of Thurston's theorem one also considers the image of multicurves by markings $\phi : S \to \widehat{\mathbb{C}}$. See also Section 1.4.
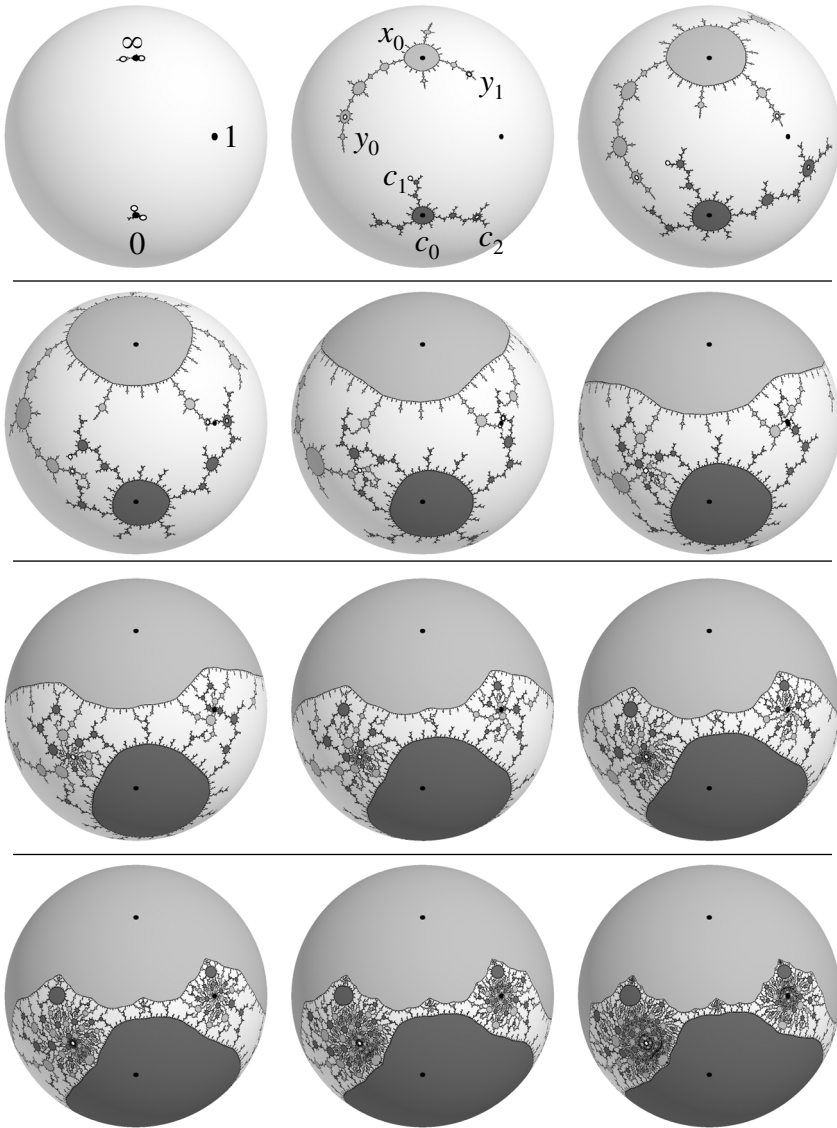
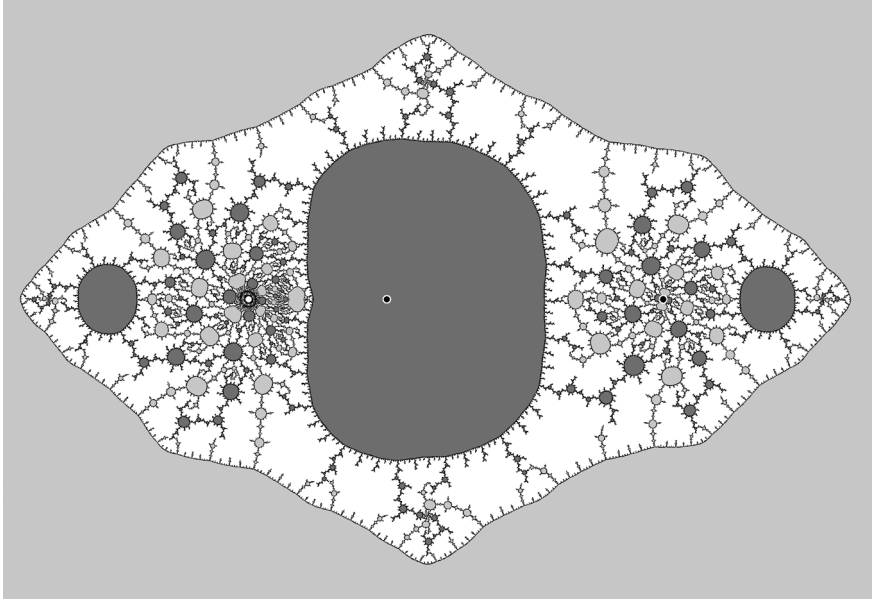Figure 17. — Sequence, centered on the middle sphere A_2. See the text for a description.
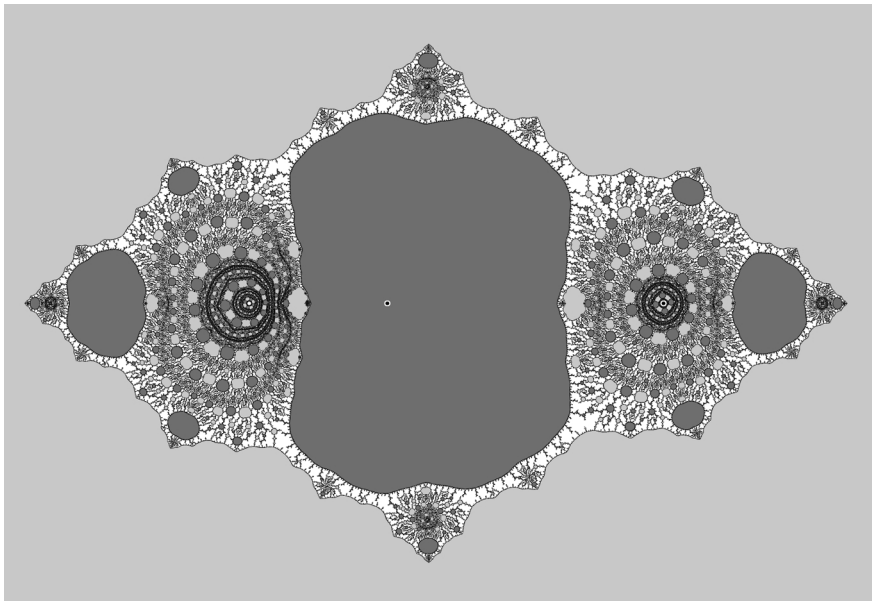
Figure 18. — Middle sphere centered flat view of $\mathcal{S}_R$ for $R = R_{10}$.

Figure 19. — Middle sphere centered flat view of $\mathcal{S}_R$ for $R = R_{15}$.
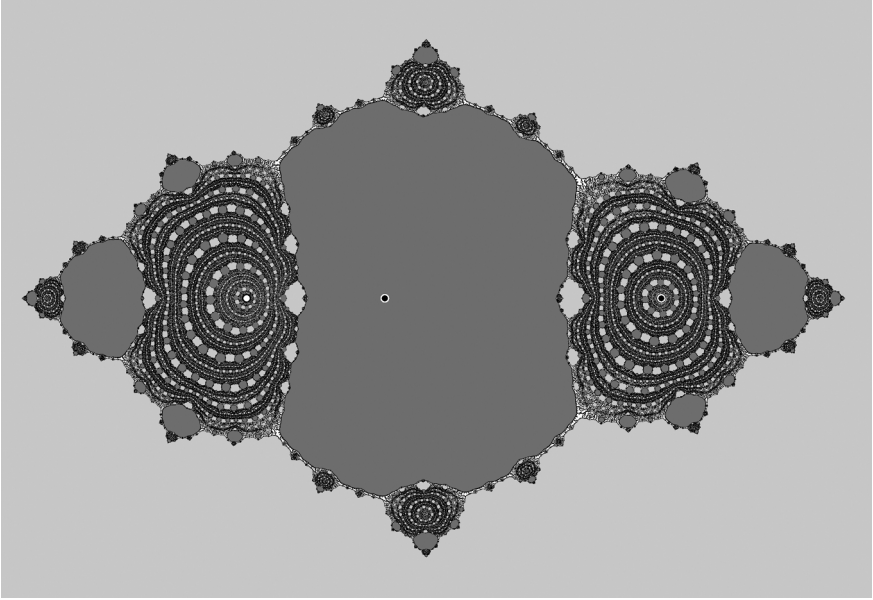
Figure 20. — Middle sphere centered flat view of $\mathcal{S}_R$ for $R = R_{20}$.

On Figure 17 we show a sequence of twelve spheres $\mathcal{S}_{R_1}$ to $\mathcal{S}_{R_{12}}$ with $R_n = 10^{4/3^n}$, which satisfies $R_{n+1}^3 = R_n$, so that each sphere maps to the previous by $F_{R_{n+1}}$; it ranges from $R_1 = 21.54\dots$ to $R_{12} = 1.0000173\dots$ The marked points and the point on the equator of argument 0, call it e_0, are highlighted as white and black dots according to a convention that we explain now: the black dots indicate the points used for the normalization of the sphere, and the white dots indicate those marked points that are not black. The normalization was chosen as follows: c_0 is sent to $0 \in \widehat{\mathbb{C}}$; x_0 is mapped to $\infty \in \widehat{\mathbb{C}}$; the point e_0 is mapped to $1 \in \widehat{\mathbb{C}}$. Hence two marked points are black. The conformal projection from $\widehat{\mathbb{C}}$ to the Euclidean sphere has been chosen so that the three black points are all visible, with 0 near the bottom, 1 on the right and ∞ near the top.

This choice of normalization is different from the ones proposed in Section 1.4. Instead of mapping three marked points to 0, 1 and ∞, we normalize so that only two marked points plus a point on the equator are mapped to 0, 1 and ∞. The reason is that for values of R that are not small, this gives a more balanced picture: indeed, if the three marked were normalized, then at least two of them would belong to one of the two polynomial. As a consequence, on the picture, only that polynomial would be visible. The drawback is that it is not obvious on which piece of the sphere cut along the short geodesics we are zooming in.
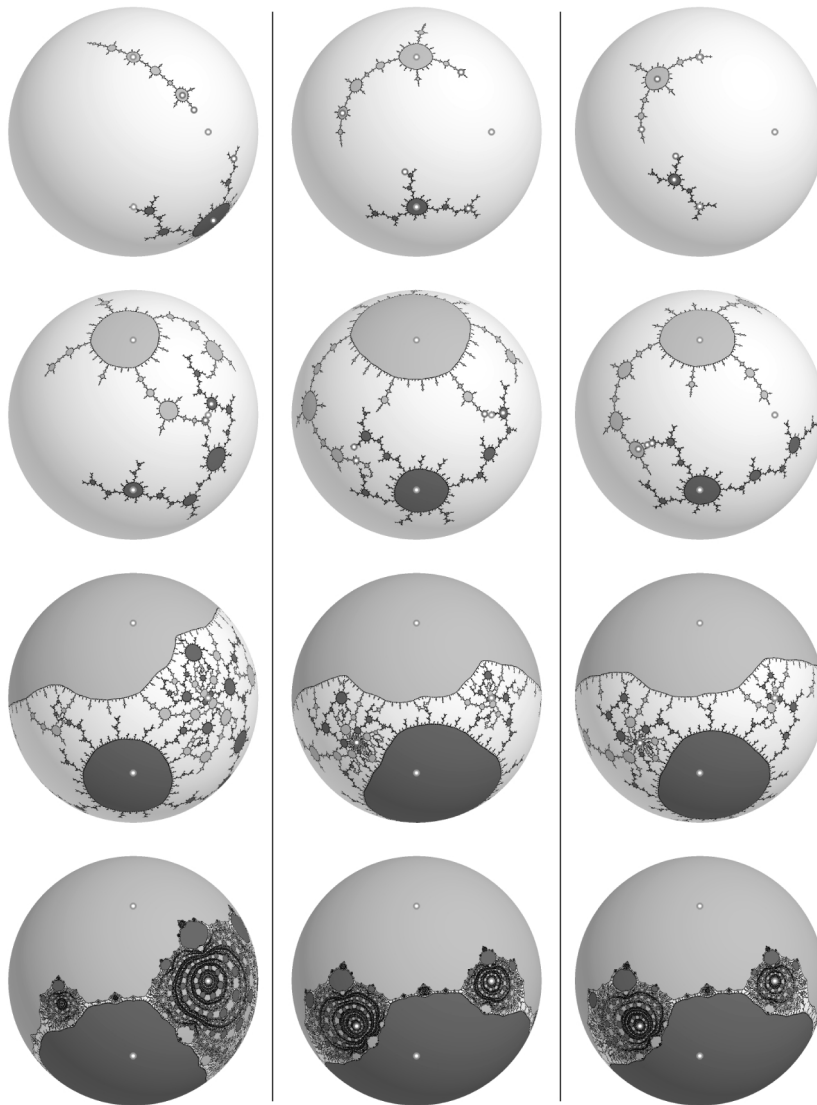
Figure 21. — Each row shows the same sphere $\mathcal{S}_R$ for $R =$ respectively R_2, R_4, R_8 and R_{16}, with $R_n = 10^{4/3^n}$. Each column has a different normalization: from left to right, (c_1, e, y_0), (c_0, e, x_0) and (c_2, e, y_1) are mapped to $(0, 1, \infty)$.

On the sequence on Figure 17, it appears that we are zooming on the middle sphere, A_2: the points y_0 and c_1 seem to gather together, like do the points y_1, c_2 and e_0. The explanation would be that in the normalizations focusing on A_3 (sending the triple y_1, c_2 and $z =$ any of the remaining four marked points to ∞, 0, 1) e_0 converges to a point distinct from the limit of the marked points (i.e. from 0, 1 and ∞).

QUESTION 1. — *Prove this assertion.*[21]

On Figures 18, 19 and 20 we drew (still conformally correct) flat views, where the black point x_0 is sent to infinity, for R_{10}, R_{15} and R_{20}.

On Figure 21 we show in parallel three sequences of four vertically stacked images, each sequence has a different normalization, each row has the same value of R. Each normalization focuses on a different piece: A_1, A_2, A_3. Notice how the middle and right column converge to a similar limit.

2.2. Interpretation of the pictures

In the three normalizations focusing on respectively A_1, A_2 and A_3, even though the family of maps F_R is supposed to diverge, the picture seems still to converge to a well defined limit, very reminiscent of a Julia set, but with mess in some Fatou components. We propose the following (conjectural) interpretation. Work of Selinger in [14] may help in giving proofs.

As $R \longrightarrow 1$, the marked sphere tends to a pack of three Riemann spheres: left, middle and right, limits of respectively A_1, A_2 and A_3, touching each other at two singular points. The map F_R has a limit $\mathcal{F}$ on this pack minus the contact points, which maps the three spheres between themselves, as rational maps. More precisely the limit $\mathcal{F}$ sends the middle sphere to the left, the left to the right, and the right back to the middle. Let us write $\mathcal{F}_1$, $\mathcal{F}_2$ and $\mathcal{F}_3$ for the three rational maps between these spheres (the domains of definition of the $\mathcal{F}_i$ include the contact points but the maps will not necessarily agree on these points, and the convergence will occur on the spheres minus these points).

On the middle sphere, the limit $\mathcal{F}_2$ has a critical point at x_0, and a double critical point at c_0. There cannot be an odd number of critical points counted with multiplicity so there must be a supplementary one. It is hiding at the contact point between the left and middle spheres. Indeed, recall that the multicurve component a has a preimage component which is homotopic to a and which is mapped $2 : 1$ to a (in an orientation reversing way). There

---

[21] For instance e_0 could be added to the set of marked points and Thurston's algorithm extended to include cycles. See the work of Selinger in [14].

is no critical point at the singular point between the middle and the right spheres, because the component of the preimage of a that is homotopic to b is sent $1:1$ to a.

The same analysis on the left sphere indicates that $\mathcal{F}_1$ has two critical points, so it has only degree 2. The critical points are y_0 and the contact point, and they respectively map to y_1 and the other contact point. Finally, the map $\mathcal{F}_3$ has no critical point. Thus the respective degrees of $\mathcal{F}_1$, $\mathcal{F}_2$, $\mathcal{F}_3$, are 2, 3, 1. Another way of seeing that would have been to look at the preimage of the nearly pinched sphere by F_R: this gives a pinched sphere with five bubbles, as on the second row of Figure 26, three of which contain the marked points (thus excluding e_0, which is not marked). Counting degrees then gives the same result.

Knowing this and the way marked points and contact points are mapped to each other, is enough, at least on the example we are studying, to completely determine the maps $\mathcal{F}_1$, $\mathcal{F}_2$, $\mathcal{F}_3$. Let us stick to the normalization used in the sequence of pictures previously shown: before the limit, map e_0 to 1 on each sphere, and the two non collapsing marked point in each sphere to 0 and ∞ for respectively P_2 and P_1. This implies in the limit that the contact point on the left sphere, the right contact point on the middle sphere, and the point e_0 on the right sphere, all map to 1 under the normalization, and that the two marked points in each sphere map to 0 and ∞ under the normalization. Then the three rational maps $\mathcal{F}_i$ must send 0 to 0, 1 to 1 and ∞ to ∞. Since moreover $\mathcal{F}_3$ has degree 1, it is the identity:

$$\mathcal{F}_3(z) = z.$$

Note that $\mathcal{F}_1$ is a polynomial and that the conjugate G_2 of $\mathcal{F}_2$ by $z \mapsto 1/z$ is polynomial (recall that a rational map is polynomial if and only if the preimage of ∞ is itself, no more, no less). The degree of G_2 is 3 and $G_2'(0) = 0$, $G_2(0) = 0$, so $G(z) = bz^3 + az^2$ with $b \neq 0$. Also $G_2(1) = 1$ so $a + b = 1$, and G_2 maps the remaining critical point $c = -2a/3b$ (whose coordinate in the middle sphere we do not know yet) to 1. This gives $4a^3 = 27b^2$. So $b = 1 - a$ and $4(a/3)^3 - a^2 + 2a - 1 = 0$. The latter equation has a double root $a = 3$ and a single root $a = 3/4$. In the case $a = 3$, we get that the other critical point $c = 1$, which we exclude: the two contact points cannot be equal. Thus $a = 3/4$, $b = 1/4$, $c = -2$ and $G_2(z) = z^2(z+3)/4$:

$$\mathcal{F}_2(z) = \frac{4z^3}{3z+1}.$$

We also got the coordinates of the left contact point on the middle sphere, which is a critical point of $\mathcal{F}_2$ and is $1/c = -1/2$. Finally, $\mathcal{F}_1$ is a degree

2 polynomial with a critical point at $z = 1$, fixing 0 and mapping 1 to the contact point on the right sphere. The latter being mapped to the contact point $-1/2$ on the middle sphere by $\mathcal{F}_3 = \mathrm{id}$ we get that $\mathcal{F}_1(1) = -1/2$.

$$\mathcal{F}_1(z) = ((z-1)^2 - 1)/2 = z^2/2 - z.$$

This is summarized on Figure 22.

QUESTION 2. — *Prove that the limit of F_R in the pinching spheres representation is indeed the map $\mathcal{F} = \mathcal{F}_1 \cup \mathcal{F}_2 \cup \mathcal{F}_3$.*
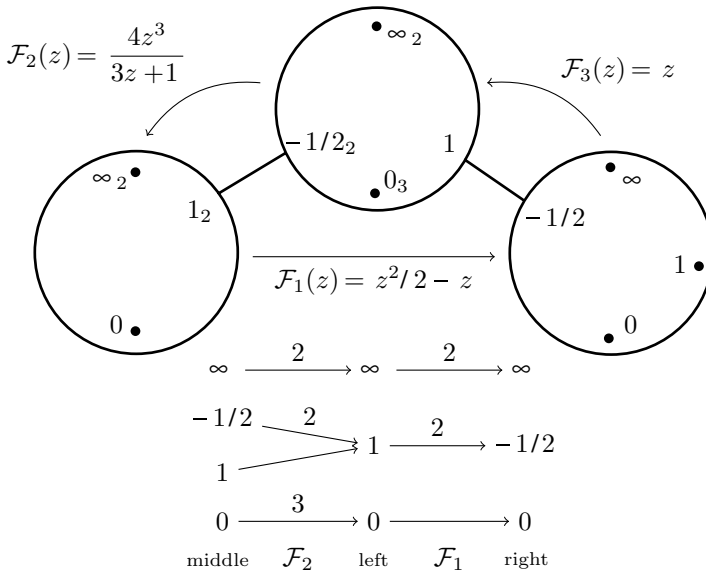

Figure 22. — Summary. Above: the subscript indicates the multiplicity of the critical points. Cross ratio of complex numbers is not respected on this schematic illustration. Below: who maps where.

Now, the third iterate of the map $\mathcal{F}$ is a map from the pack to itself which sends each sphere to itself, by three degree 6 maps that are semi-conjugate to each other because they all consist in making one turn in the following non-commutative diagram:
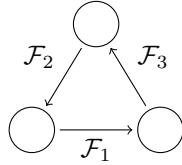
The map in the middle is $H_2 = \mathcal{F}_3 \circ \mathcal{F}_1 \circ \mathcal{F}_2$, the map on the left is $H_1 = \mathcal{F}_2 \circ \mathcal{F}_3 \circ \mathcal{F}_1$ and the map on the right is $H_3 = \mathcal{F}_1 \circ \mathcal{F}_2 \circ \mathcal{F}_3$. Since $\mathcal{F}_3$ is the identity in this example and with our choices of coordinates, we only get two different degree 6 rational maps. Let us characterize further these two maps. They both have three critical values[22]: 0, 1, ∞. The map H_2 from the middle sphere to itself has 5 critical points: $\infty \xrightarrow{4} \infty$, $1 \xrightarrow{4} 1$, $-1/2 \xrightarrow{2} -1/2$, $-1/3 \xrightarrow{2} \infty$ and $0 \xrightarrow{3} 0$, the number above the arrow indicates the local degree. The sum of "local degrees minus one" is 10, which agrees with the formula $2d - 2$ counting the number of critical points with multiplicity for a degree $d = 6$ map. The map H_1 on the left sphere has 4 critical points: $\infty \xrightarrow{4} \infty$, $1 \xrightarrow{4} 1$, $0 \xrightarrow{3} 0$, $2 \xrightarrow{3} \infty$. This is better presented as a diagram:

$$2 \xrightarrow{\ 3\ } 0 \rightleftarrows 3 \qquad\qquad\qquad 0 \rightleftarrows 3$$

$$\infty \rightleftarrows 4 \qquad\qquad -1/3 \xrightarrow{\ 2\ } \infty \rightleftarrows 4$$

$$1 \rightleftarrows 4 \qquad\qquad -1/2 \xrightarrow{\ 2\ } 1 \rightleftarrows 4$$

$$\mathcal{F}_2 \circ \mathcal{F}_3 \circ \mathcal{F}_1 \qquad\qquad \mathcal{F}_3 \circ \mathcal{F}_1 \circ \mathcal{F}_2$$
$$(= \mathcal{F}_1 \circ \mathcal{F}_2 \circ \mathcal{F}_3)$$

---

[22] In this respect they are rigid in the following sense: any rational map topologically equivalent to one of them as a ramified cover, by a pair of orientation preserving homeomorphisms, must me equivalent to it by a pair of homographies.
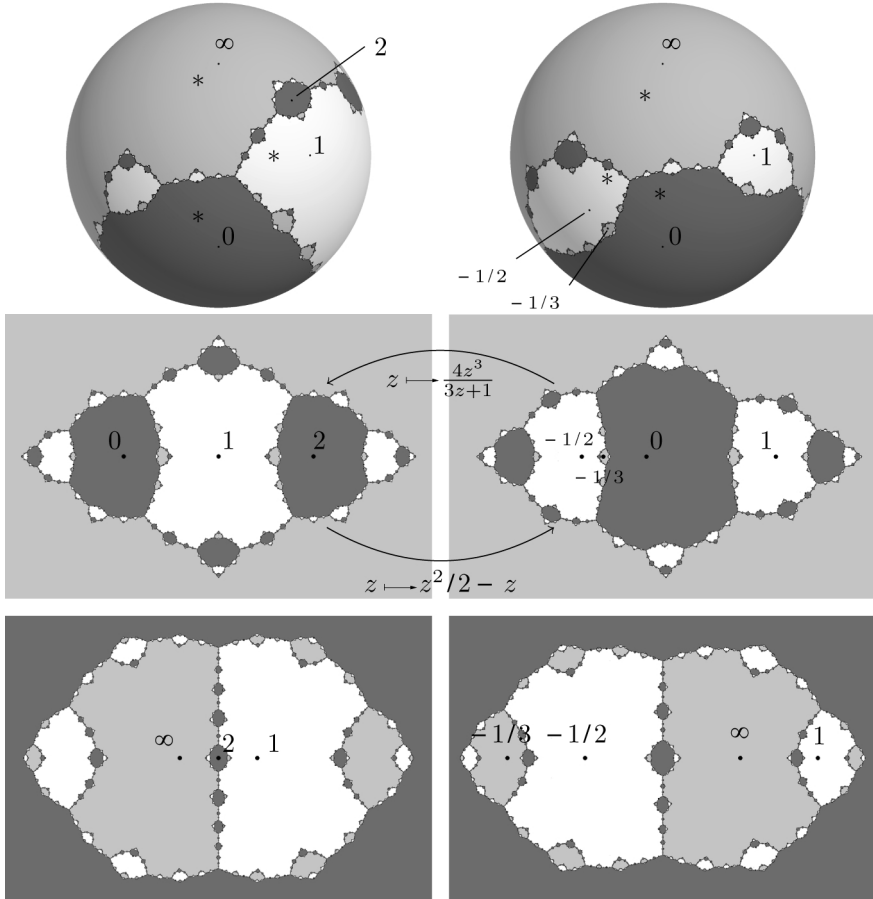
Figure 23. — Julia sets of the maps H_i (third iterate of the presumed limit on the tree of spheres). The three basins of attraction are drawn in white and shades of gray. We have put a mark "$*$" in each immediate basin in the first row. Compare with Figure 21. The column on the left represents H_1 (left sphere). The column on the right represents H_2 and H_3 (middle and right spheres). The first row is the sphere view, the second row is the flat view, and the last is the flat view followed by an inversion putting 0 at infinity. Putting the third fixed critical point at infinity would give an image identical to the second row but with a permutation of light and dark gray.

On Figure 23 are shown pictures of the Julia and Fatou sets of these two maps H_1 and H_2. For both, the behavior of the critical points and the classification of Fatou components imply that every Fatou component eventually falls under iteration in the immediate basin of one of the three fixed critical points of H_i. The picture suggests that there may be better coordinates in

which to express the H_i. For instance if one takes the coordinates $w = z - 1$ in the left sphere and $u = 1/(2z + 1)$ in the middle sphere, then we get

$$\mathcal{F}_3 \circ \mathcal{F}_1 : w \mapsto u = 1/w^2 \text{ and } \mathcal{F}_2 : u \mapsto w = -\frac{1}{u^2} \cdot \frac{u - 1/3}{1 - u/3}.$$

These are two real Blaschke fractions. So they commute with $z \mapsto \overline{z}$ and $z \mapsto 1/z$ and preserve both the real axis and the unit circle. Their compositions H_1 and H_2 have relatively simple expressions: $H_2 = \mathcal{F}_3 \circ \mathcal{F}_1 \circ \mathcal{F}_2$ reads

$$u \mapsto u^4 \left(\frac{1 - u/3}{u - 1/3} \right)^2$$

and $H_1 = \mathcal{F}_2 \circ \mathcal{F}_3 \circ \mathcal{F}_1$ reads

$$w \mapsto -w^4 \frac{1 - w^2/3}{w^2 - 1/3}.$$

Another presentation would take $s = 1 - 2/z$ in the left sphere and $t = 1 + 1/z$ in the middle sphere, and then

$$\mathcal{F}_3 \circ \mathcal{F}_1 : s \mapsto t = \frac{s + s^{-1}}{2} \text{ and } \mathcal{F}_2 : t \mapsto s = \frac{3t - t^3}{2}.$$

These are odd real maps, so they commute with $z \mapsto \overline{z}$ and $z \mapsto -z$ and preserve the real and the imaginary axis. The composition $H_1 = \mathcal{F}_2 \circ \mathcal{F}_3 \circ \mathcal{F}_1$ reads

$$s \mapsto \frac{-1}{8} \left(s^3 - 3s - \frac{3}{s} + \frac{1}{s^3} \right).$$
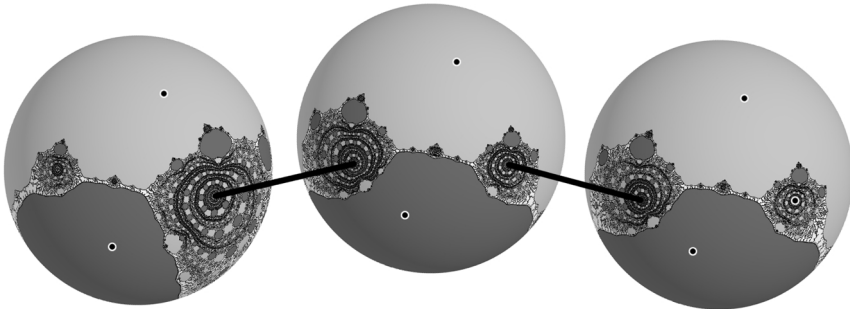

Figure 24. — The three spheres at the bottom of Figure 21, with tubes between them symbolized by black lines.

Let us show again the bottom row of Figure 21, and add black lines symbolizing the tunnels between the three spheres (one can cut little openings in each sphere and add tunnels to glue them together, and recover the inital Riemann sphere $\mathcal{S}_R$): this gives Figure 24. Comparing Figures 24 and 23, the reader will have noticed that one of the basins of the limit maps H_i is replaced by some sort of mess, that gets denser and denser as $R \to 1$. In any of the three normalizations, the Hausdorff limit of the two Julia sets seems to contain the whole basin that is white in Figure 23.

QUESTION 3. — *Prove that, in these three normalizations, the Hausdorff limit of the Julia set is indeed the union of the Julia set of H_i and of the basin of attraction that is painted white in Figure 23.*

In the next section we will focus on what happens in the tunnels between the three spheres. This may help to prove the assertion above.

2.3. Zooming on a tunnel

Up to now we observed the limits of the Julia sets in the three normalizations associated to the way the marked set degenerates. However, we could look at many other normalizations. For instance, we may focus on the tube linking the left sphere and the middle one (see Figure 16). Call it the a-tube, and call b-tube the one between the middle and right sphere. Since the left sphere is mapped to the right one and the middle to the left, the image of the a-tube has to span over the middle sphere. Recall that the map F_R is $2:1$ on the a-tube. When the a-tube is long (i.e. R is close to 1), this map is close to the squaring map $z \mapsto z^2$ in appropriate coordinates. This is why we see these square rooted copies of the central sphere image: see Figure 25. Moreover, this gets replicated by futher preimages and explains the other rings visible in Figure 25, which are more or less copies of each other by more and more square roots. Let us explain this (see also Figures 26 and 27). For a given R close to 1, the b-tube in $\mathcal{S}_{R^{1/3}}$ must contain a nearly $1:1$ copy of the a-tube for R. The square root copy of the central sphere for R found in the a-tube for $R^{1/3}$ is therefore also present in the b-tube for $R^{1/3^2}$. Now the image of the a-tube for $R^{1/3}$ not only spans over the middle sphere but also over the a-tube and b-tube for R: in fact the middle sphere represents a smaller and smaller part as $R \longrightarrow 1$. It follows that for each R, two fourth root copies of the central sphere must be found on the a-tube and two on the b-tube: these are roots of the central sphere for R^{3^k} with different values of k; however all these powers of R are close to 1 since R is. This goes on as on Figure 27 and accounts for all these rings we saw on the zoom.
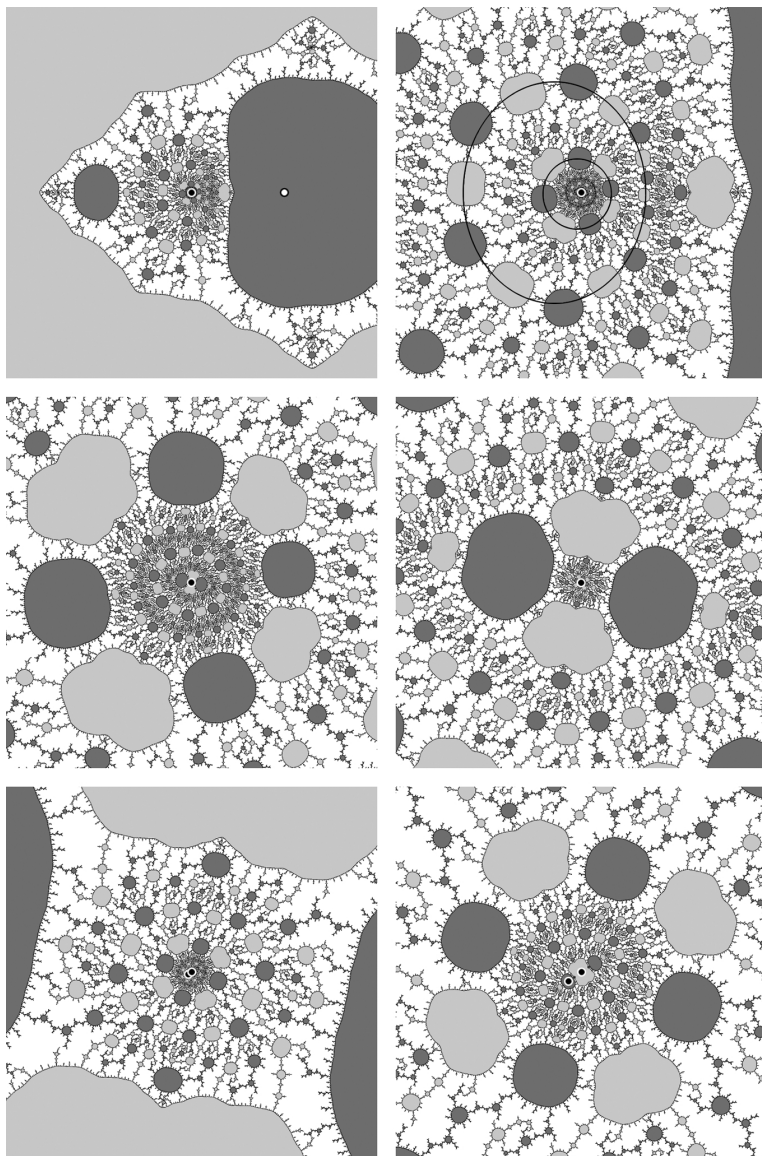
Figure 25. — A zoom on the messy part. This is a traversal of the tube starting from the middle sphere and ending at the left sphere. In the center of the last picture, we can see two white dots, which are the two marked points in the left sphere. On one picture, we also drew loops linking chains of light and dark gray components, which are approximately iterated square roots of the pictures in the middle sphere for bigger values of R.
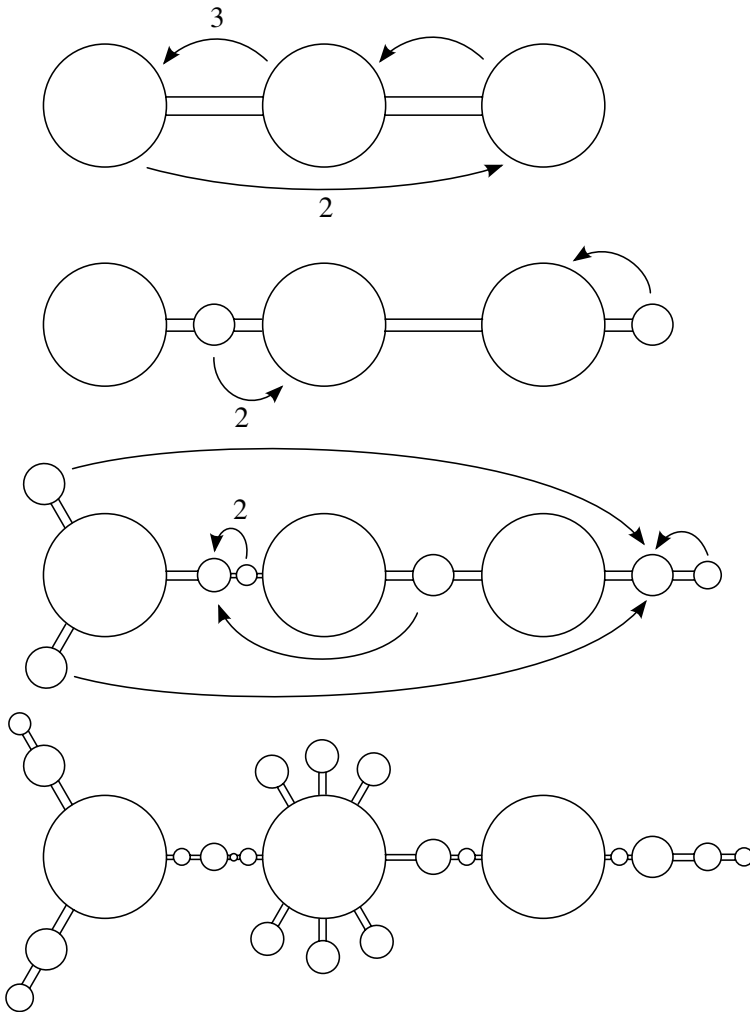
Figure 26. — Pulling back the (partially) pinched sphere tree by the maps $\mathcal{F}_R$ defines more and more pinchings. The tube between the left and the middle initial spheres gets more and more spheres, some of which separate the two inital spheres. Every sphere eventually grows antennae that strech out off the real axis.

On Figure 28 we show another conformal representation of the Riemann surfaces $\mathcal{S}_R$. These are sticks consisting of a cylinder capped with two half spheres. The length of the stick increases with n and is chosen so that we have limit pictures at the left, at the right and in the center, that are the limits of the picture in the three main normalizations as on Figure 21. The chosen normalization here puts the points on the equator with angle $1/3, 1/9, 0$ respectively to the following points on the stick: the extremal left point, the central point facing the viewer, and the extremal right point. As n increases, you will note that each end has an apparent rotation, while the central part has a non-rotating limit. Note that we also get (rotating) limits at $1/4$ and $3/4$ of the stick, and in fact at each $p/2^q$: these are the aforementioned rings of 2^q-fold preimages of the central sphere. This stick representation makes the rings and their relationships more visible. As $R \longrightarrow 1$, the rings get further and further appart from each other.
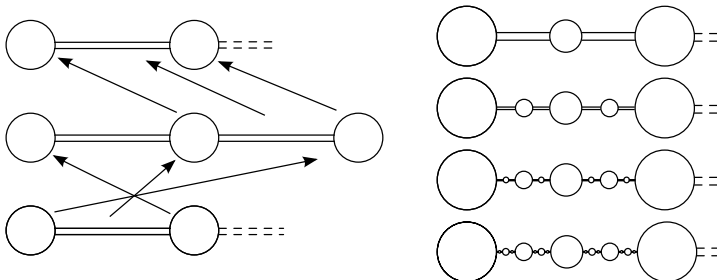

Figure 27. — Continutation of Figure 26. The spheres separating the left and middle sphere map $2 : 1$ to each other by F_R or $F_{R^3} \circ F_R$, and repeating this, eventually to the middle sphere. At the limit these separating spheres could be thought of a countable collection filling the gaps in the complement of a Cantor set.

If the tunnels on Figure 28 have a length that grows at a linear pace, which seems to be the case, then the rings also separate at a linear pace. The closer the rings, the slower the pace. When the tube is conformally mapped to a geometric sphere, say according to the central sphere normalization, this linear growth becomes an exponential shrinking: each ring in the white basin has a diameter that shrinks to 0 exponentially, with rings close to the boundary having a slower rate of convergence. More precisely for $R_n = e^{\mathrm{const}/3^n}$, the ring at $p/2^q$ should become visible when $n \geqslant \mathrm{const}\, q$ and its diameter should shrink like $e^{-\mathrm{const}\, np/2^q}$ where const designates different constants. For each q take the first $n \approx \mathrm{const}\, q$ for which the $p/2^q$ are visible: this makes rings of diameter $e^{-\mathrm{const}\, pq/2^q}$ for p from 1 to q. In particular for all $\varepsilon > 0$, when q gets big, there should be a lot of rings whose diameter is $> \varepsilon$ and with p odd, so that these rings are thin. This explains the bigger and bigger density of the distorted Julia sets $K_1(R)$ and $K_2(R)$ in the white basin as n grows.
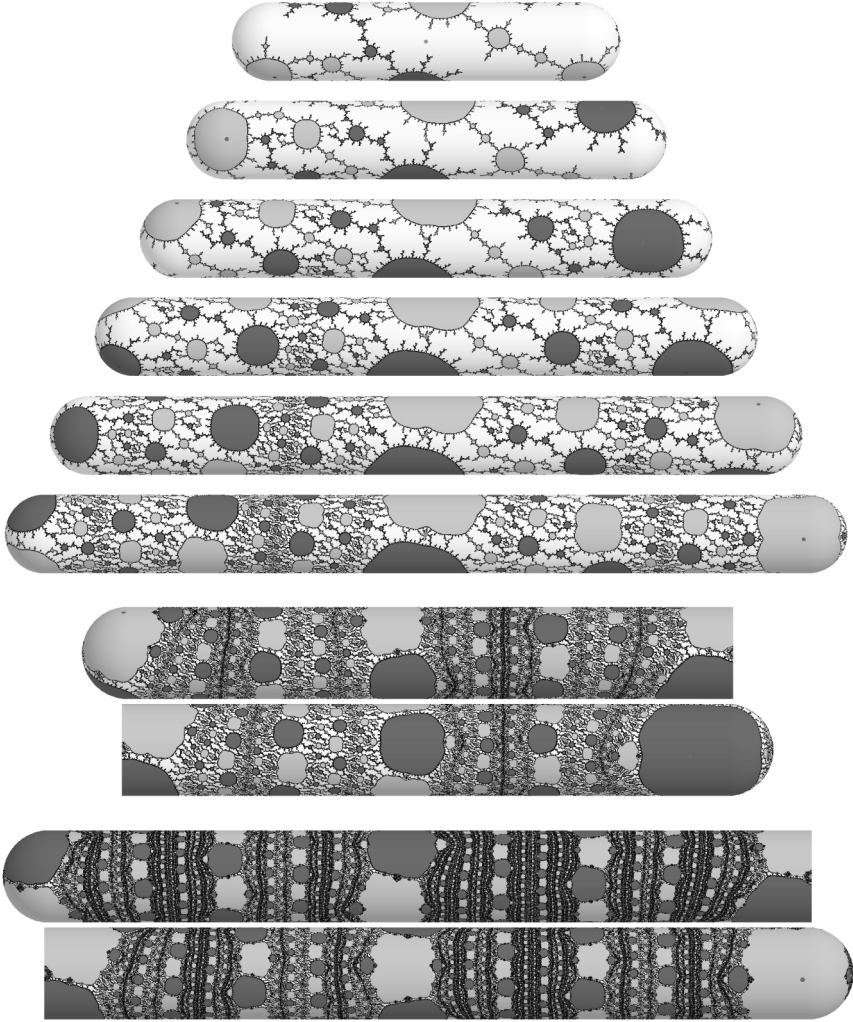
Figure 28. — Conformally correct pictures of $\mathcal{S}_R$ mapped to tubes, with $R = R_n = 10^{4/3^n}$ and $n =$ 5, 6, 7, 8, 9, 10, 13 and 16. The last two tubes were cut so as to fit in the frame. See the text for a more detailed description.

Tan Lei and Shishikura's example

n	R_n	v_n	v_n/v_{n-1}	u_n/v_n
2	2.78	1.15 $+i0.35$	0.0943 $+i0.0286$	-2.19 $+i0.48$
3	1.40	0.081 $+i0.383$	0.158 $+i0.283$	-1.49 $+i1.33$
4	1.120	-0.113 $+i0.064$	0.099 $+i0.316$	-1.15 $+i2.03$
5	1.038	-0.0324 $-i0.0230$	0.129 $+i0.276$	-1.202 $+i2.390$
10	$1+1.55e^{-4}$	$-1.16e^{-4}$ $+i0.55e^{-4}$	0.16016 $+i0.27763$	-1.38658 $+i2.40163$
15	$1+6.41e^{-7}$	$-0.36e^{-7}$ $+i4.35e^{-7}$	0.1602506 $+i0.2775626$	-1.386716 $+i2.401863$
20	$1+2.64e^{-9}$	$1.21e^{-9}$ $+i0.84e^{-9}$	0.160249937 $+i0.277561021$	-1.38672276 $+i2.40187419$
25	$1+1.08e^{-11}$	$4.51e^{-12}$ $-i2.12e^{-12}$	0.1602499527 $+i0.2775610603$	-1.386722542 $+i2.401873901$
30	$1+4.47e^{-14}$	$0.14e^{-15}$ $-i1.68e^{-14}$	0.1602499522 $+i0.2775610592$	-1.386722548 $+i2.401873910$

Table 1. — Computer experiment. Numbers rounded by truncation.

n	u_n/v_{n-1}
2	$-0.221 - i0.017$
3	$-0.615 - i0.212$
4	$-0.759 - i0.162$
5	$-0.817 - i0.023$
10	$-0.88886361 - i0.00029954$
15	$-0.88888972 - i0.00000057$
20	$-0.88888889199 - i1.46e^{-9}$
25	$-0.88888888888985 - i1.158e^{-11}$
30	$-0.8888888888888565 - i2.24e^{-14}$

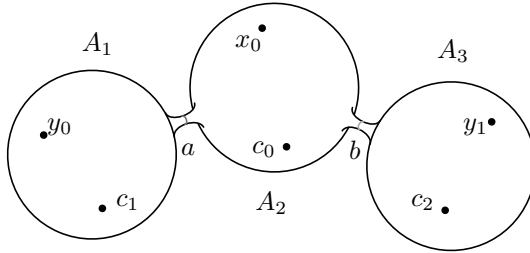Table 2. — Computer experiment. Numbers rounded by truncation.

Figure 29. — Reminder of Figure 16.

To finish, we would like to show a computer experiment measuring the rate at which the marked points group together, which is related to the rate of growth of the tubes, and the rate of shrinking of the geodesics homotopic to the canonical obstruction. Let us choose our central sphere normalization, where the points labeled c_0, e_0, x_0 are mapped respectively to $0, 1, \infty$. Let $R_n = 10^{4/3^n}$ and v_n be difference of complex coordinates from y_0 to c_1 (in the chosen normalization) and u_n from y_1 to c_2.[23] On Table 1 we list, as a function of n with $R = R_n$, the value of v_n, of the rate v_n/v_{n-1} and of the ratio u_n/v_n. The ratio u_n/v_n seems to converge: the two bunches of points converge at the same rate, which is coherent with the observation that the middle sphere is near the middle of the tubes on Figure 28 and coherent too with the fact that the tunnel in $\mathcal{S}_R$ between the middle and right sphere is a $1:1$ preimage by F_R of the other tunnel for $\mathcal{S}_{R^3}$ (growing linearly). The latter remark suggests to look at the limit of the ratio u_n/v_{n-1} and see if it is close to have absolute value one: indeed, according to Table 2, it seems to converge to $-8/9$. The rate v_n/v_{n-1} seems to tend to a complex number

$$\rho \approx 0.1602499522 + i0.277561059.$$

Putting the square of its norm in Simon Plouffe's inverter[24] suggests it might be

$$\rho \overset{?}{=} 2e^{i\pi/3}/3^{5/3}.$$

It shall not come as a surprise that the limit rate of convergence be an algebraic number: it is probably one of the eigenvalues of the fixed point of a holomorphic map with an algebraic expression. Let us explain this in more details: McMullen proved that the graph of Thurston's pull-back map

---

[23] To be very precise, if $\phi_1[R]$, $\phi_2[R]$ and $\phi_3[R]$ from S to $\widehat{\mathbb{C}}$ denote the three normalization, with ϕ_1 for the left normalization, ϕ_2 for the middle one and ϕ_3 for the right one, then $v_n = \phi_2[R_n](c_1) - \phi_2[R_n](y_0)$ and $u_n = \phi_2[R_n](c_2) - \phi_2[R_n](y_1)$.

[24] Available on the Internet at http://pi.lacim.uqam.ca/ as of January 2012.

projects to a subset of the graph of an algebraic correspondence on the moduli space, with algebraic coefficients, see [6]. Selinger proved that Thurston's pull-back map extends continuously to the Weil-Petersson completion of the Teichmüller space, see [14]. The latter projects to a natural compactification of moduli space: the Deligne-Mumford compactification, which is a complex smooth algebraic variety. The correspondence extends to this compactification (though it may have an indeterminacy locus in some parts); it has a fixed point corresponding to the tree of three spheres; it has a branch defined near this fixed point, that is possibly ramified, in which case: a blow up is necessary, the fixed point on the exceptional divisor must be identified and the map must be studied near this new fixed point. Then we expect the map to be regular near the fixed point and one of its eigenvalues to be the limit rate of convergence.

QUESTION 4. — *Carry out these computations, compute this eigenvalue, prove it is equal to the limit rate of convergence of the points, and compare its value to the one conjectured above.*

Even though from Table 1, $R_n - 1$ and v_n seem to decrease to 0 at the same rate, we expect one to tend slightly faster: $R_n - 1 \sim \ln(10)/3^n$ whereas $v_n \sim$ constant ρ^n for the value of ρ given above, and $|\rho| = 0.320\ldots \neq 1/3 = 0.333\ldots$

3. Acknowledgments

Bibliography

[1]   BUFF (X.), FEHRENBACH (J.), LOCHAK (P.), SCHNEPS (L.) and VOGEL (P.). — Moduli spaces of curves, mapping class groups and fields theory, volume 9 of SMF/AMS Texts and Monographs. American Mathematical Society, Providence, RI (2003). Translated from the French by Schneps.

[2]   BUFF (X.), EPSTEIN (A. L.) and KOCH (S.). — Twisted matings and equipotential gluings, Ann. Fac. Sci. Toulouse Math (6), 21(5), (2012).

[3] BUFF (X.), EPSTEIN (A. L.), MEYER (D.), PILGRIM (K. M.), REES (M.) and TAN (L.). — Questions about polynomial matings, Ann. Fac. Sci. Toulouse Math (6), 21(5), (2012).

[4] DOUADY (A.) and HUBBARD (J. H.). — A proof of Thurston's topological characterization of rational functions. Acta Math., 171(2) p. 263-297 (1993).

[5] HUBBARD (J. H.). — Teichmüller theory and applications to geometry, topology, and dynamics. Vol. 1. Matrix Editions, Ithaca, NY (2006). Teichmüller theory, With contributions by Adrien Douady, William Dunbar, Roland Roeder, Sylvain Bonnot, David Brown, Allen Hatcher, Chris Hruska and Sudeb Mitra, With forewords by William Thurston and Clifford Earle.

[6] KOCH (S.). — A new link between Teichmüller theory and complex dynamics (PhD thesis). PhD thesis, Cornell Univ. (2008).

[7] LEVY (S.). — Critically Finite Rational Maps (PhD thesis). PhD thesis, Princeton Univ. (1985).

[8] MEYER (D.), PETERSEN (C. L.). — On the Notion of Matings, Ann. Fac. Sci. Toulouse Math (6), 21(5), (2012).

[9] MILNOR (J.). — Geometry and dynamics of quadratic rational maps. Experiment. Math., 2(1) p. 37-83 (1993). With an appendix by the author and Lei Tan.

[10] MILNOR (J.). — Pasting together Julia sets: a worked out example of mating. Experiment. Math., 13(1) p. 55-92 (2004).

[11] PILGRIM (K. M.). — Canonical Thurston obstructions. Adv. Math., 158(2) p. 154-168 (2001).

[12] PILGRIM (K.). — An algebraic formulation of Thurston's characterization of rational functions, Ann. Fac. Sci. Toulouse Math (6), 21(5), (2012).

[13] REES (M.). — A partial description of parameter space of rational maps of degree two. I. Acta Math., 168(1-2) p. 11-87 (1992).

[14] SELINGER (N.). — Thurston's pullback map on the augmented Teichmüller space and applications. arXiv:1010.1690v2.

[15] SHISHIKURA (M.). — On a theorem of M. Rees for matings of polynomials. In The Mandelbrot set, theme and variations, volume 274 of London Math. Soc. Lecture Note Ser., p. 289-305. Cambridge Univ. Press, Cambridge (2000).

[16] SHISHIKURA (M.) and TAN (L.). — A family of cubic rational maps and matings of cubic polynomials. Experiment. Math., 9(1) p. 29-53 (2000).